INTERNATIONAL JOURNAL FOR NUMERICAL METHODS IN FLUIDS
Int. J. Numer. Meth. Fluids 2005; **49**:1359–1389
Published online 23 August 2005 in Wiley InterScience (www.interscience.wiley.com). DOI: 10.1002/fld.1031

A general optimal formulation for the dynamic Smagorinsky subgrid-scale stress model

Bing-Chen Wang[1,‡] and Donald J. Bergstrom[2,*,†]

[1]*Defence R&D Canada–Suffield, P.O. Box 4000, Medicine Hat, AB, Canada T1A8K6*
[2]*Department of Mechanical Engineering, University of Saskatchewan, Saskatoon, SK, Canada S7N5A9*

SUMMARY

In this paper, a general optimal formulation for the dynamic Smagorinsky subgrid-scale (SGS) stress model is reported. The Smagorinsky constitutive relation has been revisited from the perspective of functional variation and optimization. The local error density of the dynamic Smagorinsky SGS model has been minimized directly to determine the model coefficient C_S. A sufficient and necessary condition for optimizing the SGS model is obtained and an orthogonal condition (OC), which governs the instantaneous spatial distribution of the optimal dynamic model coefficient, is formulated. The OC is a useful general optimization condition, which unifies several classical dynamic SGS modelling formulations reported in the literature. In addition, the OC also results in a new dynamic model in the form of a Picard's integral equation. The approximation tensorial space for the projected Leonard stress is identified and the physical meaning for several basic grid and test-grid level tensors is systematically discussed. Numerical simulations of turbulent Couette flow are used to validate the new model formulation as represented by the Picard's integral equation for Reynolds numbers ranging from 1500 to 7050 (based on one half of the velocity difference of the two plates and the channel height). The relative magnitudes of the Smagorinsky constitutive parameters have been investigated, including the model coefficient, SGS viscosity and filtered strain rate tensor. In general, this paper focuses on investigation of fundamental mathematical and physical properties of the popular Smagorinsky constitutive relation and its related dynamic modelling optimization procedure. Copyright © 2005 John Wiley & Sons Ltd.

KEY WORDS: large eddy simulation; subgrid-scale model; constitutive relation; optimization; turbulence

*Correspondence to: Donald J. Bergstrom, Department of Mechanical Engineering, University of Saskatchewan, Saskatoon, SK, Canada S7N5A9.
†E-mail: don_bergstrom@engr.usask.ca, http://www.interscience.wiley.com/jpages/0271-2091/
‡E-mail: bingchen.wang@drdc-rddc.gc.ca

Contract/grant sponsor: Natural Sciences and Engineering Research Council

Received 7 January 2005
Accepted 25 May 2005

1. INTRODUCTION

Interest in the application of large eddy simulation (LES) to turbulent flows has been renewed in the past decade. One significant improvement was the development of so-called dynamic models. In the context of Smagorinsky-type subgrid-scale (SGS) models, the assumption of a SGS viscosity is adopted to relate the SGS stress to the filtered strain rate tensor. The dynamic Smagorinsky model (SM) of Germano *et al.* [1] is based on an innovation which uses a second test-grid filter to dynamically extract modelling information from the resolved scales of motion to determine the model coefficient C_S. Traditionally, C_S is regarded in the most general case as a function of time and space. However, the system of equations to be used for calculating it is overdetermined and does not admit a unique solution. Practical implementation of such dynamic SMs has instead relied on the use of the theory of optimization to determine the 'best' instantaneous spatial distribution for C_S.

Using the least squares method, Lilly [2] proposed a modified optimal formulation for the dynamic model (DM) of Germano *et al.* [1]. The constitutive relation (Smagorinsky) for the DM is based on the Boussinesq assumption, which admits a linear relation between the resolved strain rate tensor and the SGS stress to be modelled. Recently, the optimal DM formulation obtained by Lilly has been extended from a linear to a dynamic nonlinear quadratic form by Wang and Bergstrom [3, 4] following the stress modelling approach via explicit tensorial polynomial expansion introduced by Lumley [5], Pope [6], and Lund and Novikov [7]. Previous optimal LES modelling approaches also include the so-called ideal LES formulations proposed by Langford and Moser [8] and Zandonade *et al.* [9], which aim to reproduce all single-time, multipoint statistics accurately and minimize the error of large-scale dynamics via stochastic approximations. The dynamic localization Smagorinsky SGS stress model of Ghosal *et al.* [10] was based on minimizing a residual functional, which is an integral of the norm of the residual tensor of the Germano identity over the entire domain. They obtained a Fredholm integral equation of the second kind (FIE2), which determines the optimal spatial distribution of the model coefficient and avoids the mathematical inconsistency encountered in the conventional DM of Germano *et al.* [1] and Lilly [2]. By introducing the SGS kinetic energy transport equation (k-equation) and using a similar variational method, Ghosal *et al.* [10] reformulated their integral equation and developed a new dynamic localization model. The latter reformulated model prohibits instability due to the occasional excessive backscatter of the SGS energy and is weakly realizable with $k \geqslant 0$. Making use of the observation that C_S is a fairly slowly varying function of time, Piomelli and Liu [11] proposed an approximate extrapolation scheme to localize the dynamic SM. Although their approximate method is not rigorously compatible with variational theory, it has the benefit of avoiding the large cost in CPU time required for solving the FIE2, and has been successfully tested using a rotating channel flow. Menon *et al.* [12], Kim and Menon [13], and Pallares and Davidson [14] tested a different k-equation dynamic localization model, which is based on the similarity behaviour observed in the experiment of Liu *et al.* [15] and the least squares method of optimization adopted by Lilly [2]. Carati *et al.* [16] developed a dynamic localization stochastic model by introducing an eddy force term into the SGS model to account for the backscatter of SGS kinetic energy. Similar to the approach of Ghosal *et al.* [10], Carati *et al.* [16] achieved the goal of optimization by minimizing a globally integrated residual. A common feature of the global optimization technique is that it minimizes the residual integrated over the general domain (usually an integral-type functional), which does not necessarily ensure that the local

residual is minimal. One of the objectives of this paper is to minimize the local residual directly, avoiding such a global integration and yet maintaining mathematical consistency.

Notwithstanding the alternative approaches discussed above [3, 4, 12–14, 16], the dynamic Smagorinsky-type models remain the most popular in LES, and this paper focuses on exploring the properties of this type of models in terms of the constitutive relation and the optimization technique used for the dynamic modelling procedure. Before introducing the new approach of optimization, it is necessary to review the previous contributions of Germano *et al.* [1], Lilly [2], and Ghosal *et al.* [10]. In LES, the flow variables are decomposed into a resolved large-scale component (denoted by an overbar) and a SGS component using a filtering technique, i.e.

$$\bar{\phi}(\mathbf{x}) = \int_{-\infty}^{\infty} \phi(\mathbf{y}) G(\mathbf{x}, \mathbf{y})\, \mathrm{d}\mathbf{y} \tag{1}$$

where $G(\mathbf{x}, \mathbf{y})$ represents the convolution kernel associated with a characteristic filter size $\bar{\Delta}$. By applying the filtering process to the momentum equation for incompressible flow, the SGS stress tensor of the grid level appears as

$$\tau_{ij} = \overline{u_i u_j} - \bar{u}_i \bar{u}_j \tag{2}$$

which then needs to be modelled to represent the effect of the SGS motions on the resolved field.

1.1. *Conventional dynamic Smagorinsky SGS model* [1, 2]

The conventional Smagorinsky-type dynamic SGS model introduced by Germano *et al.* [1] and modified by Lilly [2] was a breakthrough and has been widely used for LES. In their model, the constitutive relation between the grid level SGS stress and the resolved strain rate tensor can be expressed as

$$\tau_{ij}^* = \tau_{ij} - \frac{\delta_{ij}}{3}\tau_{kk} = -2C_{\mathrm{S}}\bar{\Delta}^2 |\bar{S}| \bar{S}_{ij} \tag{3}$$

The asterisk is used to indicate the trace-free form of a tensor and δ_{ij} is the Kronecker delta. The resolved strain rate tensor has the form of $\bar{S}_{ij} = \frac{1}{2}(\bar{u}_{i,j} + \bar{u}_{j,i})$ and its magnitude is evaluated by $|\bar{S}| = (2\bar{S}_{ij}\bar{S}_{ij})^{1/2}$. The test-grid level SGS stress tensor is defined as

$$T_{ij} = \widetilde{\overline{u_i u_j}} - \tilde{\bar{u}}_i \tilde{\bar{u}}_j \tag{4}$$

where the tilde represents the test-grid filtering process based on a characteristic filter size of $\tilde{\bar{\Delta}}$. Similar to the approach for τ_{ij}^*, the constitutive relation between T_{ij}^* and $\tilde{\bar{S}}_{ij}$ can be modelled as

$$T_{ij}^* = T_{ij} - \frac{\delta_{ij}}{3}T_{kk} = -2C_{\mathrm{S}}\tilde{\bar{\Delta}}^2 |\tilde{\bar{S}}| \tilde{\bar{S}}_{ij} \tag{5}$$

The two SGS stresses, i.e. τ_{ij} and T_{ij}, are related by the Germano identity [1], defined as

$$\mathscr{L}_{ij} = T_{ij} - \tilde{\tau}_{ij} \tag{6}$$

where $\mathscr{L}_{ij}$ is the resolved Leonard-type stress: $\mathscr{L}_{ij} = \widetilde{\bar{u}_i \bar{u}_j} - \tilde{\bar{u}}_i \tilde{\bar{u}}_j$. Substituting Equations (3) and (5) into the trace-free form of Equation (6), the following equation is obtained:

$$\mathscr{L}^*_{ij} = -\alpha_{ij} C_S + \widetilde{\beta_{ij} C_S} \tag{7}$$

where

$$\alpha_{ij} = 2\tilde{\bar{\Delta}}^2 |\tilde{\bar{S}}| \tilde{\bar{S}}_{ij} \tag{8}$$

$$\beta_{ij} = 2\bar{\Delta}^2 |\bar{S}| \bar{S}_{ij} \tag{9}$$

At any specific spatial position, Equation (7) represents five independent instantaneous equations for the single unknown, C_S. Therefore, Equation (7) is an overdetermined system, and consequently a unique solution for C_S is not available and a residual exists between the right- and left-hand sides of Equation (7). However, an optimal value for C_S can be obtained by minimizing the *local error density function*, which, at each time step, is a function of space defined by

$$Q = E_{ij} E_{ij} \tag{10}$$

where E_{ij} is the *local error tensor*, based on the residual of Equation (7), i.e.

$$E_{ij} = \mathscr{L}^*_{ij} + \alpha_{ij} C_S - \widetilde{\beta_{ij} C_S} \tag{11}$$

From the theory of approximation [17], we know that the above optimization approach seeks the projection of $\mathscr{L}^*_{ij}$ in the specified approximation tensor space of the model, $\mathfrak{M}_L^{\text{orig}}$ (which will be discussed later in Section 3). The projection then represents the 'best substitute' for $\mathscr{L}^*_{ij}$, i.e.

$$\mathscr{L}^*_{ij} \approx \mathscr{L}^{\text{proj}^*}_{ij} = -\alpha_{ij} C_S^{\aleph} + \widetilde{\beta_{ij} C_S^{\aleph}} \tag{12}$$

where the superscript $\aleph$ represents the optimal result. From the above concepts and Equation (11), the local error tensor takes the following form:

$$E_{ij} = \mathscr{L}^*_{ij} - \mathscr{L}^{\text{proj}^*}_{ij} \tag{13}$$

The difficulty in minimizing Q comes from the filtered term in Equation (11), i.e. $\widetilde{\beta_{ij} C_S}$. Germano *et al.* [1] and Lilly [2] both used an assumption of incomplete spatial invariance (ISI), which assumes C_S to be spatially invariant so that it can be extracted from this filtering operation; whereas, C_S is assumed to be spatially variant in the other parts of the model. Therefore, a mathematical inconsistency emerges, i.e. the treatment of C_S in the second and third terms on the right-hand side of Equation (11) is different. Nevertheless, with this assumption, Equation (11) can be simplified to

$$E_{ij} = \mathscr{L}^*_{ij} + M_{ij} C_S \tag{14}$$

where

$$M_{ij} = \alpha_{ij} - \tilde{\beta}_{ij} \tag{15}$$

The physical meaning of α_{ij}, β_{ij}, M_{ij} and $\mathscr{L}_{ij}^{\text{proj}^*}$ will be proposed in Section 2. Minimizing Q using the least squares method and noting that the trace of $\mathscr{L}_{ij}$ vanishes, then yields the conventional DM formula first derived by Lilly [2]

$$C_{\text{S}}^{\aleph}(\mathbf{x}) = -\frac{M_{ij}\mathscr{L}_{ij}}{M_{ij}M_{ij}} \tag{16}$$

It has been observed that the above popular DM formulation can lead to an unrealistic SGS dissipation effect if the model coefficient is restricted to be positive; on the other hand, a potential numerical instability arises due to excessive backscatter of the SGS turbulent kinetic energy (TKE) if the model coefficient is allowed to be negative [11, 18]. Furthermore, the model is not bounded and admits a possible singularity when the denominator of the formulation ($M_{ij}M_{ij}$) becomes very small [18, 19]. Finally, this model is based on the classical Boussinesq assumption which requires the principal axes of the negative SGS stress tensor to be aligned with those of the resolved strain rate tensor, and thus leads to an inadequate tensorial geometrical representation of the SGS stress [3, 20]. To prevent the potential numerical insatiability, plane averaging technique is often applied to the modelling formula (16) when 2-D homogeneity exists [1, 11, 18, 21, 22]. The drawbacks of the Smagorinsky-type models addressed above are related to the overly simplified linear Boussinesq constitutive relation. Recent dynamic nonlinear modelling approaches [3, 4, 7, 23–25] have demonstrated some significant improvement related to these issues.

Also, it should be indicated that the above optimization procedure to obtain Equation (16) is based on the minimal residual of the Germano identity, which was the first and is still the most popular criterion in the dynamic SGS modelling procedure. However, it is not the only choice. Other criteria involving different types of identities include: the kinetic energy identity originally introduced by Cabot and utilized by Ghosal *et al.* [10], a new identity involving an explicit filter and its inverse by Kuerten *et al.* [26], the generalized Germano identity by Sagaut [19], and the vector identity by Morinishi and Vasilyev [27]. The Germano identity began to attract scrutiny right after the classical papers of Germano *et al.* [1] and Lilly [2] were published. Some relevant research papers include Ronchi *et al.* [28], Meneveau and Katz [29], Kuerten *et al.* [26], and Brun and Friedrich [30]. Using Taylor series expansions, Brun and Friedrich [30] extensively studied the grid level SGS stress tensor τ_{ij}, test-grid level SGS stress tensor T_{ij} and Germano identity. The errors involved in the SGS stress terms were specified in their study and the corresponding corrections to the stress terms have been quantified.

1.2. Global functional optimization approach [10]

On observing the mathematical inconsistency in the conventional DM mentioned above, Ghosal *et al.* [10] minimized a global error functional using the functional variational method without adopting the *a priori* assumption of ISI to handle $\widetilde{\beta_{ij}C_{\text{S}}}$. The global error functional adopted in their approach is defined as

$$\mathscr{F}(C_{\text{S}}) = \int_{-\infty}^{\infty} Q \, \mathrm{d}\mathbf{x} = \int_{-\infty}^{\infty} E_{ij}E_{ij} \, \mathrm{d}\mathbf{x} \tag{17}$$

To find the 'best' spatial distribution of C_S, such that the global error functional $\mathscr{F}$ is minimal, the variation of $\mathscr{F}$ must vanish, i.e.

$$\delta\mathscr{F}(C_S, \delta C_S) = 2\int_{-\infty}^{\infty} E_{ij}[\alpha_{ij}\delta C_S - \widetilde{\beta_{ij}\delta C_S}]\mathrm{d}\mathbf{x} = 0 \tag{18}$$

which then results in the following integral equation:

$$\alpha_{ij}(\mathbf{x})E_{ij}(\mathbf{x}) - \beta_{ij}(\mathbf{x})\int_{-\infty}^{\infty} E_{ij}(\mathbf{y})G(\mathbf{y},\mathbf{x})\,\mathrm{d}\mathbf{y} = 0 \tag{19}$$

This equation can be further rewritten in the form of a FIE2 with a non-singular kernel if $\alpha_{ij}(\mathbf{x})\alpha_{ij}(\mathbf{x}) \neq 0$. In the approach of Ghosal *et al.* [10], a global integration in Equation (17) is necessary to extract the function δC_S from the filtering term $\widetilde{\beta_{ij}\delta C_S}$, so that Equation (19) can be obtained using the functional variational theory. However, as will be shown in Section 2, we have found that the local error density function Q can be minimized *directly* by introducing the Dirac delta function without adopting such an additional global integration. Numerical results for turbulent Couette flow based on the new approach will be presented in Section 4. The major conclusion of the paper will be summarized in Section 5.

2. A SUFFICIENT AND NECESSARY CONDITION FOR LOCAL OPTIMIZATION OF THE DYNAMIC SMAGORINSKY MODEL

Although some approximate local optimization methods are available, e.g. the conventional DM [2] based on the assumption of ISI and the integral-type localization model obtained by minimizing the integral of Q over the entire domain [10], a consistent mathematical method for minimizing Q directly is not yet available in the literature. The philosophical idea for finding such a direct consistent local optimization approach is borrowed from solid mechanics, which utilizes the Dirac delta function $\delta_D(\mathbf{x},\mathbf{y})$ as an important tool to treat local effects (e.g. the local concentrated non-continuous forces and moments), so that they can be generally included in the continuous differential or integral governing equations and be treated in the same way as other globally continuous effects or forces.

In order to find the extremum value of Q directly using the functional variational method following the above idea, it is necessary to redefine the quantities E_{ij} and Q. We use the symbols $\mathscr{E}_{ij}$ and $\mathscr{Q}$ to indicate their modified definitions, respectively. The modified definition for the local error tensor, which is analogous to Equation (11), takes the following form:

$$\mathscr{E}_{ij}(\mathbf{x},\mathbf{x}_0) = \mathscr{L}^*_{ij}(\mathbf{x}_0) + \alpha_{ij}(\mathbf{x}_0)C_S(\mathbf{x},\mathbf{x}_0) - \int_{-\infty}^{\infty}\beta_{ij}(\mathbf{y})C_S(\mathbf{y},\mathbf{x}_0)G(\mathbf{x}_0,\mathbf{y})\,\mathrm{d}\mathbf{y} \tag{20}$$

where $C_S(\mathbf{x},\mathbf{x}_0)$ and $\mathscr{E}_{ij}(\mathbf{x},\mathbf{x}_0)$ represent, respectively, the model coefficient function and local error tensor function of $\mathbf{x}$ for a *specific* location $\mathbf{x}_0$. The variable $\mathbf{x}$ runs over the entire computational domain (Σ) and these two 3-D spatial functions are specific for the given location $\mathbf{x}_0 \in \Sigma$. The local error density retains a similar form to Equation (10), however, it becomes a functional of $C_S(\mathbf{x},\mathbf{x}_0)$, using the following fixed point mapping:

$$\mathscr{Q}(C_S(\mathbf{x}_0,\mathbf{x}_0)) = \mathscr{E}_{ij}(\mathbf{x},\mathbf{x}_0)\mathscr{E}_{ij}(\mathbf{x},\mathbf{x}_0)|_{\mathbf{x}=\mathbf{x}_0} \tag{21}$$

which varies only with the coefficient function $C_S(\mathbf{x}, \mathbf{x}_0)$ at a given location $\mathbf{x}_0$. The variational problem then can be defined as follows: at the location $\mathbf{x}_0 \in \Sigma$, find an optimal function $C_S^{\aleph}(\mathbf{x}, \mathbf{x}_0) \in \Upsilon$ such that $\mathscr{Q}(C_S^{\aleph}(\mathbf{x}_0, \mathbf{x}_0))$ is minimal. Here, $C_S^{\aleph}(\mathbf{x}_0, \mathbf{x}_0)$ is the localization (optimal) model coefficient and Υ represents the function space for $C_S(\mathbf{x}, \mathbf{x}_0)$. All $C_S^{\aleph}(\mathbf{x}, \mathbf{x}_0)$ for different locations generate a *set of optimal coefficient functions*, i.e.

$$\{C_S^{\aleph}\} = \{C_S^{\aleph}(\mathbf{x}, \mathbf{x}_0) \mid \mathscr{Q}(C_S^{\aleph}(\mathbf{x}_0, \mathbf{x}_0)) \leqslant \mathscr{Q}(C_S(\mathbf{x}_0, \mathbf{x}_0)),\ \forall\, C_S(\mathbf{x}, \mathbf{x}_0) \in \Upsilon,\ \forall\, \mathbf{x}_0 \in \Sigma\} \tag{22}$$

and all $C_S^{\aleph}(\mathbf{x}_0, \mathbf{x}_0)$, $\forall\, \mathbf{x}_0 \in \Sigma$, generate a *set of optimal model coefficients*, which taken together represent a 3-D optimal distribution of C_S, i.e.

$$\{C_S^{\aleph 0}\} = \{C_S^{\aleph}(\mathbf{x}_0, \mathbf{x}_0) \mid \mathscr{Q}(C_S^{\aleph}(\mathbf{x}_0, \mathbf{x}_0)) \leqslant \mathscr{Q}(C_S(\mathbf{x}_0, \mathbf{x}_0)),\ \forall\, C_S(\mathbf{x}, \mathbf{x}_0) \in \Upsilon,\ \forall\, \mathbf{x}_0 \in \Sigma\} \tag{23}$$

which retains a function mapping (surjective) from the spatial domain Σ to the image set $\{C_S^{\aleph 0}\}$. Thus, unlike the traditional approach of searching for one optimal function $C_S(\mathbf{x})$ for the entire domain at each time step, the new approach will look for the optimal function set and the set of optimal model coefficients, i.e. $\{C_S^{\aleph}\}$ and $\{C_S^{\aleph 0}\}$, respectively. These two sets are *uncountable* in the continuous case, while having at least N^3 independent elements in the discrete case, where N^3 represents the total number of discrete nodes. Although conceptually more abstract than the traditional approach, this new mathematical approach of regarding the model coefficient C_S does not change its role in determining the SGS stress defined by Equation (3) within the classical framework of the Smagorinsky constitutive relation, and as will be shown later, it is actually more flexible in terms of mathematics. Furthermore, some general formulations and useful physical concepts can be derived using this new approach.

With the redefined mathematical expressions for $\mathscr{E}_{ij}(\mathbf{x}, \mathbf{x}_0)$, $\mathscr{Q}(C_S(\mathbf{x}_0, \mathbf{x}_0))$, $\{C_S^{\aleph}\}$, and $\{C_S^{\aleph 0}\}$, we can begin the regular procedure of optimization for the variational problem defined previously. Let the first order variation of $\mathscr{Q}$ vanish, i.e.

$$\delta \mathscr{Q} = 2\mathscr{E}_{ij}\delta\mathscr{E}_{ij} = 0 \tag{24}$$

$\forall\, \mathbf{x}_0 \in \Sigma$. Considering Equations (20) and (21), the above equation becomes

$$\mathscr{E}_{ij}(\mathbf{x}_0, \mathbf{x}_0)\left[\alpha_{ij}(\mathbf{x}_0)\delta C_S(\mathbf{x}_0, \mathbf{x}_0) - \int_{-\infty}^{\infty} \beta_{ij}(\mathbf{y})\delta C_S(\mathbf{y}, \mathbf{x}_0) G(\mathbf{x}_0, \mathbf{y})\, \mathrm{d}\mathbf{y}\right] = 0 \tag{25}$$

The Dirac delta function $\delta_D(\mathbf{x}, \mathbf{y})$ has the property: $\phi(\mathbf{x}) = \int_{-\infty}^{\infty} \phi(\mathbf{y})\delta_D(\mathbf{x}, \mathbf{y})\, \mathrm{d}\mathbf{y}$, such that Equation (25) can be expressed as

$$\int_{-\infty}^{\infty} \mathscr{E}_{ij}(\mathbf{x}_0, \mathbf{x}_0)[\alpha_{ij}(\mathbf{y})\delta_D(\mathbf{x}_0, \mathbf{y}) - \beta_{ij}(\mathbf{y})G(\mathbf{x}_0, \mathbf{y})]\delta C_S(\mathbf{y}, \mathbf{x}_0)\, \mathrm{d}\mathbf{y} = 0 \tag{26}$$

$\forall\, \delta C_S(\mathbf{y}, \mathbf{x}_0) \in \Upsilon$. Therefore, the following relation must hold:

$$\mathscr{E}_{ij}(\mathbf{x}_0, \mathbf{x}_0)[\alpha_{ij}(\mathbf{y})\delta_D(\mathbf{x}_0, \mathbf{y}) - \beta_{ij}(\mathbf{y})G(\mathbf{x}_0, \mathbf{y})] = 0 \tag{27}$$

$\forall\, \mathbf{x}_0 \in \Sigma$, or more briefly

$$\mathscr{E}_{ij}M'_{ij} = 0 \tag{28}$$

where $\mathscr{E}_{ij} = \mathscr{E}_{ij}(\mathbf{x}_0, \mathbf{x}_0)$, and

$$M'_{ij} = M'_{ij}(\mathbf{y}, \mathbf{x}_0) = \alpha_{ij}(\mathbf{y})\delta_{\mathrm{D}}(\mathbf{x}_0, \mathbf{y}) - \beta_{ij}(\mathbf{y})G(\mathbf{x}_0, \mathbf{y}) \tag{29}$$

Because of the Dirac delta function contained in its first term, M'_{ij} is a generalized tensorial function [31] of $\mathbf{y}$ at a given location $\mathbf{x}_0$. In view of the convolution contained in $\mathscr{E}_{ij}$ (see Equation (20)), Equation (28) is actually an integral equation with respect to $C_{\mathrm{S}}(\mathbf{x}, \mathbf{x}_0)$. Equation (28) also indicates an elegant *orthogonal condition* (OC) between the local residual stress (or error stress tensor) $\mathscr{E}_{ij}$ and the tensor M'_{ij} at any given location $\mathbf{x}_0$. So far, the OC has been proven to be a necessary condition for making the functional $\mathscr{Q}$ minimal and as such represents a Distribution Equation for the local optimal model Coefficient (DEC) for the dynamic Smagorinsky SGS stress model. In effect, this OC is also a sufficient condition for minimizing $\mathscr{Q}$, and the proof of sufficiency will be addressed at the end of this section.

The following is an attempt to provide an interpretation of the previously discussed tensors M'_{ij} and $\mathscr{L}_{ij}^{\mathrm{proj}^*}$, and also tensors α_{ij} and β_{ij} which are frequently encountered in the literature. In order to understand the physical meaning of these tensors, we need to revisit some basic concepts given in Section 1.1. From the constitutive relation given by Equation (3), we understand that at each time step, β_{ij} acts as the '*base stress tensor function*' (explicit function of space) for the grid level SGS stress τ^*_{ij}, which is then obtained by weighting β_{ij} with $(-C_{\mathrm{S}})$. Similarly, α_{ij} can be interpreted as the '*base stress tensor function*' for the test-grid level SGS stress T^*_{ij} at each time step. Both α_{ij} and β_{ij} are related to the filtered stain rate tensor $\bar{S}_{ij}$. Extensive discussions on $\bar{S}_{ij}$-related tensorial integrity bases, invariants and the tensorial spaces for the Reynolds stress and SGS stress, can be found in References [3–7, 23, 24, 32–34]. Recall that the Leonard stress term $\mathscr{L}^*_{ij}$ in the Germano identity (Equation (6)) is approximated by Equation (12) using the SGS models given by Equations (3) and (5). Equation (12) indicates that $\mathscr{L}^*_{ij}$ is approximated using α_{ij} and β_{ij} by a linear weighting operation involving $C_{\mathrm{S}}^{\aleph}(\mathbf{x}, \mathbf{x}_0)$. From the definition of M'_{ij}, the following interesting constructive relation between $\mathscr{L}_{ij}^{\mathrm{proj}^*}$ and M'_{ij} can be readily obtained:

$$\mathscr{L}_{ij}^{\mathrm{proj}^*}(\mathbf{x}_0) = -\int_{-\infty}^{\infty} C_{\mathrm{S}}^{\aleph}(\mathbf{y}, \mathbf{x}_0) M'_{ij}(\mathbf{y}, \mathbf{x}_0)\, \mathrm{d}\mathbf{y} \tag{30}$$

$\forall\, \mathbf{x}_0 \in \Sigma$. From the point of view of approximation theory, the variational problem defined previously can be equivalently expressed as follows: at a given location $\mathbf{x}_0$, find $C_{\mathrm{S}}^{\aleph}(\mathbf{x}, \mathbf{x}_0) \in \Upsilon$ for the projection of $\mathscr{L}^*_{ij}(\mathbf{x}_0)$ in the specified approximation stress tensor space $\mathfrak{M}_{\mathrm{o}}$, i.e. $\mathscr{L}_{ij}^{\mathrm{proj}^*}(\mathbf{x}_0) \in \mathfrak{M}_{\mathrm{o}}$, such that the 'error', $\mathscr{E}_{ij}(\mathbf{x}_0, \mathbf{x}_0)$, is orthogonal to $\mathfrak{M}_{\mathrm{o}}$ (see Equation (28)). Here, $\mathfrak{M}_{\mathrm{o}}$ is a *local approximation tensor space for the Leonard stress at* $\mathbf{x}_0$, constructed by

$$\begin{aligned} \mathfrak{M}_{\mathrm{o}} &= \mathfrak{M}_{\mathrm{o}}(\mathbf{x}_0) \\ &= \left\{ \mathscr{L}_{ij}^{\mathrm{appr}^*}(\mathbf{x}_0) \,\middle|\, \mathscr{L}_{ij}^{\mathrm{appr}^*}(\mathbf{x}_0) = -\int_{-\infty}^{\infty} C_{\mathrm{S}}(\mathbf{y}, \mathbf{x}_0) M'_{ij}(\mathbf{y}, \mathbf{x}_0)\, \mathrm{d}\mathbf{y},\ \forall\, C_{\mathrm{S}}(\mathbf{y}, \mathbf{x}_0) \in \Upsilon, \mathbf{y} \in \Sigma \right\} \end{aligned} \tag{31}$$

Obviously, $\mathscr{L}_{ij}^{\mathrm{appr}^*}(\mathbf{x}_0)$, the *element of the local approximation tensor space for the Leonard stress*, is a functional of $C_{\mathrm{S}}(\mathbf{y}, \mathbf{x}_0)$ at the location $\mathbf{x}_0 \in \Sigma$, and the space $\mathfrak{M}_{\mathrm{o}}$ is specific for $\mathbf{x}_0$.

The above variational problem requires that $\mathscr{E}_{ij}(\mathbf{x}_0,\mathbf{x}_0)$ be orthogonal to any element in $\mathfrak{M}_o$, which can be validated in a straightforward manner using Equations (28) and (31):

$$\mathscr{E}_{ij}(\mathbf{x}_0,\mathbf{x}_0)\mathscr{L}_{ij}^{\text{appr}^*}(\mathbf{x}_0) = -\int_{-\infty}^{\infty} C_S(\mathbf{y},\mathbf{x}_0)\mathscr{E}_{ij}(\mathbf{x}_0,\mathbf{x}_0)M'_{ij}(\mathbf{y},\mathbf{x}_0)\,d\mathbf{y} \equiv 0 \tag{32}$$

$\forall \mathscr{L}_{ij}^{\text{appr}^*}(\mathbf{x}_0) \in \mathfrak{M}_o$.

Equation (31) shows a linear constructive relation between $\mathscr{L}_{ij}^{\text{appr}^*}(\mathbf{x}_0)$ and M'_{ij}, weighted by $C_S(\mathbf{y},\mathbf{x}_0)\,d\mathbf{y}$ in a 3-D continuous case. Considering the difference in units between $\mathscr{L}_{ij}^{\text{appr}^*}(\mathbf{x}_0)$ and M'_{ij}, M'_{ij} can thus be understood as the '*intensity tensor function*' of the local elementary approximation Leonard stress $\mathscr{L}_{ij}^{\text{appr}^*}(\mathbf{x}_0)$. Equation (31) also profoundly demonstrates how in a dynamic SM approach, the *local* elementary approximation Leonard stress $\mathscr{L}_{ij}^{\text{appr}^*}(\mathbf{x}_0)$ is constructed through the *local* test-grid level SGS stress and the *global* grid level SGS stress. Since $\alpha_{ij}(\mathbf{x}_0) = \int_{-\infty}^{\infty} \alpha_{ij}(\mathbf{y})\delta_D(\mathbf{x}_0,\mathbf{y})\,d\mathbf{y}$, the first term of M'_{ij}, i.e. $\alpha_{ij}(\mathbf{y})\delta_D(\mathbf{x}_0,\mathbf{y})$ in Equation (29), reflects the contribution of the *local* test-grid level stress (indicated by α_{ij}) to the local value of $\mathscr{L}_{ij}^{\text{appr}^*}(\mathbf{x}_0)$ because of the sharp localization effect of the Dirac Delta function at $\mathbf{x}_0$. Similarly, the second term, $\beta_{ij}(\mathbf{y})G(\mathbf{x}_0,\mathbf{y})$, reflects the contribution of the grid level stress (indicated by β_{ij}) at *all locations* to the local value of $\mathscr{L}_{ij}^{\text{appr}^*}(\mathbf{x}_0)$ using the filter kernel function $G(\mathbf{x}_0,\mathbf{y})$ as a weight at $\mathbf{x}_0$.

Since the reversed procedure from Equation (27) to Equation (24) also strictly holds, the OC (Equation (28)) is equivalent to the variational condition (Equation (24)). In mathematics [35], the variational condition (Equation (24)) is regarded as a necessary condition for the functional minimization. However, since $\mathscr{Q} = \mathscr{E}_{ij}\mathscr{E}_{ij}$ is a second order functional of $C_S(\mathbf{x},\mathbf{x}_0)$ and is non-negative, the value of $\mathscr{Q}$ can only be minimal for the optimal local coefficient function. Details of the proof of sufficiency are given in Appendix A. Thus, the variational condition (Equation (24)) and the OC (Equation (28)) are not only necessary but also sufficient for minimizing the local error functional $\mathscr{Q}$. This is the principal conclusion of this research work, which can be briefly summarized by the following proposition:

Proposition

For the dynamic Smagorinsky SGS stress model, the local error density functional $\mathscr{Q}$ at a given location $\mathbf{x}_0$, is minimum, if and only if $\mathscr{E}_{ij}M'_{ij} = 0$.

3. PRELIMINARY THEORETICAL APPLICATIONS OF THE OC

In this and the following sections, some preliminary theoretical and numerical applications of the above-obtained sufficient and necessary condition (the OC) for optimizing the dynamic SM will be presented, respectively. The applications and examples to be presented in these two sections serve the purpose of demonstrating how to utilize the OC to derive some useful practical results. However, it should be indicated that these applications and examples are not intended to be a complete demonstration of the properties of the OC and its potential applications; a full theoretical and numerical exploration of the topic is beyond the scope of this paper.

In the remainder of this section, we present three theoretical derivatives of the OC, i.e.: using the OC to derive the conventional dynamic SGS stress modelling formula of Lilly [2], the dynamic model of Ghosal *et al.* [10] in the form of a FIE2, and a new dynamic optimal SGS model in the form of a Picard's integral equation (PIE).

Integrating both sides of the OC in terms of $\mathbf{y}$ over the entire domain, results in

$$\mathscr{E}_{ij}(\mathbf{x}_0, \mathbf{x}_0)[\alpha_{ij}(\mathbf{x}_0) - \tilde{\beta}_{ij}(\mathbf{x}_0)] = 0 \tag{33}$$

$\forall\, \mathbf{x}_0 \in \Sigma$. Applying the definition of M_{ij} given in Equation (15), the above relation simplifies to

$$\mathscr{E}_{ij} M_{ij} = 0 \tag{34}$$

which is the *integral form of the orthogonal condition* (IOC) at any given location $\mathbf{x}_0$. M_{ij} is another frequently encountered tensor in the literature, which in view of the previous discussion, can be explained in general terms as the difference between the test-grid level SGS base stress and the filtered grid level SGS base stress, i.e. $\alpha_{ij} - \tilde{\beta}_{ij}$. Although an additional integration has been performed in obtaining Equation (33) from the OC, the result still retains some implications of the original variational problem, which now requires the local error tensor $\mathscr{E}_{ij}$ to be orthogonal to M_{ij} at a given location $\mathbf{x}_0$. An elegant linear constructive relation between M'_{ij} and M_{ij} can be obtained from Equation (29) as follows

$$M_{ij}(\mathbf{x}_0) = \int_{-\infty}^{\infty} M'_{ij}\, \mathrm{d}\mathbf{y} \tag{35}$$

at a given location $\mathbf{x}_0$. The application of the above equation will be demonstrated in Section 3.1.

Substituting $\mathscr{E}_{ij}$ as defined in Equation (20) into the IOC, we obtain

$$\mathscr{L}^*_{ij}(\mathbf{x}_0) M_{ij}(\mathbf{x}_0) + \alpha_{ij}(\mathbf{x}_0) M_{ij}(\mathbf{x}_0) C_{\mathrm{S}}(\mathbf{x}_0, \mathbf{x}_0) - M_{ij}(\mathbf{x}_0) \int_{-\infty}^{\infty} \beta_{ij}(\mathbf{y}) C_{\mathrm{S}}(\mathbf{y}, \mathbf{x}_0) G(\mathbf{x}_0, \mathbf{y})\, \mathrm{d}\mathbf{y} = 0 \tag{36}$$

which is an integral equation that governs the optimal function $C^{\aleph}_{\mathrm{S}}(\mathbf{x}, \mathbf{x}_0)$ at any given location $\mathbf{x}_0$. However, this is not a regular integral equation in that $C^{\aleph}_{\mathrm{S}}(\mathbf{x}, \mathbf{x}_0)$ can in principle be different at every $\mathbf{x}_0$, which means that the integral equation needs to be solved at all N^3 discrete nodes for the independent optimal functions. In general, this would be costly and is of little practical interest. Fortunately, some useful special solutions of Equation (36) under specific restrictions have been found, e.g. the DM of Lilly [2], the FIE2 of Ghosal *et al.* [10] and a new modelling formula in the form of a PIE to be derived in the remainder of this section.

3.1. Restriction to constant distribution of $C^{\aleph}_{\mathrm{S}}(\mathbf{x}, \mathbf{x}_0)$

If $C^{\aleph}_{\mathrm{S}}(\mathbf{x}, \mathbf{x}_0) \equiv C^{\aleph}_{\mathrm{S}}(\mathbf{x}_0, \mathbf{x}_0)$, i.e. $C^{\aleph}_{\mathrm{S}}(\mathbf{x}, \mathbf{x}_0)$ has a 3-D spatially constant distribution with respect to $\mathbf{x}$ at each $\mathbf{x}_0$, $\{C^{\aleph}_{\mathrm{S}}\}$ then becomes a set consisting of independent constant functions. Thus Equation (36) becomes

$$[\mathscr{L}^*_{ij}(\mathbf{x}_0) + M_{ij}(\mathbf{x}_0) C^{\aleph}_{\mathrm{S}}(\mathbf{x}_0, \mathbf{x}_0)] M_{ij}(\mathbf{x}_0) = 0 \tag{37}$$

which then results in

$$C_S^{\aleph}(\mathbf{x}_0, \mathbf{x}_0) = -\frac{M_{ij}(\mathbf{x}_0)\mathscr{L}_{ij}(\mathbf{x}_0)}{M_{ij}(\mathbf{x}_0)M_{ij}(\mathbf{x}_0)} \tag{38}$$

$\forall\, \mathbf{x}_0 \in \Sigma$. Clearly, the above result obtained using the revised approach is the same as the conventional DM formulation of Lilly [2], i.e. Equation (16), except for the conceptual difference that here we are looking for an optimal coefficient set $\{C_S^{\aleph 0}\}$ instead of the conventional single optimal coefficient function $C_S^{\aleph}(\mathbf{x})$. However, this conceptual difference does not result in any difference between Equation (16) and Equation (38) in calculating the value of the local DM coefficient in any numerical tests. The constant functions are independent (and can be different) at each different $\mathbf{x}_0$, such that $\{C_S^{\aleph 0}\}$ can still yield a non-constant optimal distribution of the model coefficient over the entire 3-D domain. As such, it has been demonstrated that the conventional assumption of ISI is not the only way to obtain Lilly's result. From the above approach, we now understand that Lilly's result can be generalized as a special solution of the IOC. The restriction condition of the new approach based on the set $\{C_S^{\aleph 0}\}$ is weaker than the conventional [1, 2] assumption of ISI, and thus provides a method for obtaining Lilly's result in a mathematically consistent way. This is due to the fact that in comparison with the conventional approach [1, 2] for a single optimal function $C_S^{\aleph}(\mathbf{x})$, the new approach has the advantage of allowing the freedom to choose an independent optimal function at each position to compose $\{C_S^{\aleph 0}\}$.

An alternative consistent approach to obtain Lilly's formulation can start from the construction equation for $\mathscr{L}_{ij}^{\mathrm{proj}^*}$, i.e. Equation (30). Under the restriction condition considered, i.e. $C_S^{\aleph}(\mathbf{x}, \mathbf{x}_0) \equiv C_S^{\aleph}(\mathbf{x}_0, \mathbf{x}_0)$, $C_S^{\aleph}(\mathbf{x}, \mathbf{x}_0)$ is independent of $\mathbf{x}$ at a given location $\mathbf{x}_0$. Therefore, using Equation (35), Equation (30) becomes

$$\mathscr{L}_{ij}^{\mathrm{proj}^*}(\mathbf{x}_0) = -C_S^{\aleph}(\mathbf{x}_0, \mathbf{x}_0)M_{ij}(\mathbf{x}_0) \tag{39}$$

which has a specific meaning in physics, i.e. under the restriction condition of $C_S^{\aleph}(\mathbf{x}, \mathbf{x}_0) \equiv C_S^{\aleph}(\mathbf{x}_0, \mathbf{x}_0)$, the projected Leonard stress $\mathscr{L}_{ij}^{\mathrm{proj}^*}(\mathbf{x}_0)$ can be generated from the tensor $M_{ij}(\mathbf{x}_0)$ using the coefficient $-C_S^{\aleph}(\mathbf{x}_0, \mathbf{x}_0)$ as a weight. From the theory of approximation, an orthogonal relation must exist between $\mathscr{E}_{ij}$ and $\mathscr{L}_{ij}^{\mathrm{proj}^*}(\mathbf{x}_0)$, i.e. $\mathscr{E}_{ij}\mathscr{L}_{ij}^{\mathrm{proj}^*}(\mathbf{x}_0) = 0$ or

$$-[\mathscr{L}_{ij}^{*}(\mathbf{x}_0) - \mathscr{L}_{ij}^{\mathrm{proj}^*}(\mathbf{x}_0)]C_S^{\aleph}(\mathbf{x}_0, \mathbf{x}_0)M_{ij}(\mathbf{x}_0) = 0 \tag{40}$$

The above equation yields two solutions, i.e. a trivial solution of $C_S^{\aleph}(\mathbf{x}_0, \mathbf{x}_0) \equiv 0$, and an orthogonal relation of $[\mathscr{L}_{ij}^{*}(\mathbf{x}_0) - \mathscr{L}_{ij}^{\mathrm{proj}^*}(\mathbf{x}_0)]M_{ij}(\mathbf{x}_0) = 0$ which upon substituting Equation (39) results in Equations (37) and (38), the revised conventional dynamic SGS model of Lilly [2] proposed previously. Therefore, besides the general interpretation given at the beginning of Section 3, $M_{ij}(\mathbf{x}_0)$ can be further identified from Equation (39) as the '*base stress tensor*' for the local elementary approximation Leonard stress $\mathscr{L}_{ij}^{\mathrm{appr}^*}(\mathbf{x}_0)$ in the specific case of the revised conventional dynamic SGS modelling approach (Equation (38)) considered. Thus, under the restriction of $C_S^{\aleph}(\mathbf{x}, \mathbf{x}_0) \equiv C_S^{\aleph}(\mathbf{x}_0, \mathbf{x}_0)$, the revised conventional dynamic approach of Lilly [2] seeks $C_S^{\aleph}(\mathbf{x}_0, \mathbf{x}_0)$ to generate $\mathscr{L}_{ij}^{\mathrm{proj}^*}(\mathbf{x}_0)$ in the local approximation tensor space

constructed by

$$\mathfrak{M}_{\mathrm{L}}^{\mathrm{rev}} = \mathfrak{M}_{\mathrm{L}}^{\mathrm{rev}}(\mathbf{x}_0)$$
$$= \{\mathscr{L}_{ij}^{\mathrm{appr}^*}(\mathbf{x}_0) | \mathscr{L}_{ij}^{\mathrm{appr}^*}(\mathbf{x}_0) = -C_{\mathrm{S}}(\mathbf{x}_0, \mathbf{x}_0) M_{ij}(\mathbf{x}_0),\ \forall\, C_{\mathrm{S}}(\mathbf{x}_0, \mathbf{x}_0) \in \mathfrak{R}\} \tag{41}$$

where $\mathfrak{R}$ is the set of real numbers. Clearly, $\mathfrak{M}_{\mathrm{L}}^{\mathrm{rev}} \subseteq \mathfrak{M}_{\mathrm{o}}$ at $\mathbf{x}_0$. Again, it should be noted that the above interpretation of Lilly's approximation tensor space for the Leonard stress is mathematically consistent because Equation (39) is obtained from Equation (30) without resorting to the assumption of ISI. However, if we use the original assumption [1, 2] of ISI and begin from Equation (14), we can obtain the original approximation tensor function space of Lilly [2] for the Leonard stress, following a similar analysis, i.e.

$$\mathfrak{M}_{\mathrm{L}}^{\mathrm{orig}} = \{\mathscr{L}_{ij}^{\mathrm{appr}^*}(\mathbf{x}) | \mathscr{L}_{ij}^{\mathrm{appr}^*}(\mathbf{x}) = -C_{\mathrm{S}}(\mathbf{x}) M_{ij}(\mathbf{x}),\ \forall\, C_{\mathrm{S}}(\mathbf{x}) \in \mathscr{C}(\Sigma),\ \mathbf{x} \in \Sigma\} \tag{42}$$

where $\mathscr{C}(\Sigma)$ represents the set of continuous functions over the domain Σ. It is easy to show that in this specific case of Lilly's original approach [2], the orthogonal relation is $E_{ij}(\mathbf{x}) M_{ij}(\mathbf{x}) = 0$, and similarly, $M_{ij}(\mathbf{x})$ serves as the '*base stress tensor function*' for $\mathscr{L}_{ij}^{\mathrm{appr}^*}(\mathbf{x})$ weighted by $-C_{\mathrm{S}}(\mathbf{x})$. Thus far, the construction of the elementary approximation Leonard stress has been interpreted for both the original [2] and current revised dynamic SGS stress modelling formula, and the application of Equation (35) for relating M_{ij} and M'_{ij} has also been demonstrated.

3.2. *Restriction to identical distribution of* $C_{\mathrm{S}}^{\aleph}(\mathbf{x}, \mathbf{x}_0)$

3.2.1. A new Picard's integral equation. If $C_{\mathrm{S}}^{\aleph}(\mathbf{x}, \mathbf{x}_0)$ has the same 3-D spatial distribution for each $\mathbf{x}_0$, the elements of the set $\{C_{\mathrm{S}}^{\aleph}\}$ become identical, i.e. $C_{\mathrm{S}}^{\aleph}(\mathbf{x}, \mathbf{x}_a) \equiv C_{\mathrm{S}}^{\aleph}(\mathbf{x}, \mathbf{x}_b)$, $\forall \mathbf{x} \in \Sigma$ and $\mathbf{x}_a \neq \mathbf{x}_b$. This simplifies the problem to the traditional approach of searching for a single optimal coefficient function $C_{\mathrm{S}}^{\aleph}(\mathbf{x})$ over the entire domain, instead of a special optimal function $C_{\mathrm{S}}^{\aleph}(\mathbf{x}, \mathbf{x}_0)$ for each $\mathbf{x}_0$. This is a desirable feature and Equation (36) becomes a regular integral equation, which is a Fredholm integral equation of the third kind (FIE3) or PIE [36], i.e.

$$\mathscr{L}_{ij}^{*}(\mathbf{x}) M_{ij}(\mathbf{x}) + \alpha_{ij}(\mathbf{x}) M_{ij}(\mathbf{x}) C_{\mathrm{S}}(\mathbf{x}) - M_{ij}(\mathbf{x}) \int_{-\infty}^{\infty} \beta_{ij}(\mathbf{y}) C_{\mathrm{S}}(\mathbf{y}) G(\mathbf{x}, \mathbf{y})\, \mathrm{d}\mathbf{y} = 0 \tag{43}$$

where the replacement of $\mathbf{x}_0$ by $\mathbf{x}$ is valid, since the equation holds $\forall\, \mathbf{x}_0 \in \Sigma$. In the case of $\alpha_{ij}(\mathbf{x}) M_{ij}(\mathbf{x}) \neq 0$, this FIE3 or the PIE can be further rearranged into a new FIE2:

$$f(\mathbf{x}) = C_{\mathrm{S}}(\mathbf{x}) + \int_{-\infty}^{\infty} \psi(\mathbf{x}, \mathbf{y}) C_{\mathrm{S}}(\mathbf{y})\, \mathrm{d}\mathbf{y} \tag{44}$$

where

$$f(\mathbf{x}) = -\frac{\mathscr{L}_{ij}^{*}(\mathbf{x}) M_{ij}(\mathbf{x})}{\alpha_{ij}(\mathbf{x}) M_{ij}(\mathbf{x})} \tag{45}$$

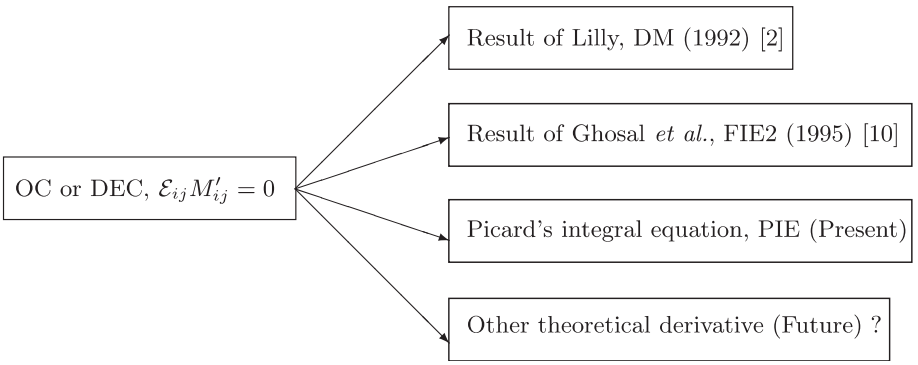

Figure 1. Direct theoretical applications of the OC.

and the non-symmetric kernel is

$$\psi(\mathbf{x},\mathbf{y})=-\frac{M_{ij}(\mathbf{x})\beta_{ij}(\mathbf{y})}{\alpha_{ij}(\mathbf{x})M_{ij}(\mathbf{x})}G(\mathbf{x},\mathbf{y}) \tag{46}$$

3.2.2. Fredholm integral equation of the second kind of Ghosal et al. [*10*]. The above integral equations, i.e. Equations (43) and (44) were obtained using the IOC, which is different than the FIE2 obtained by Ghosal *et al.* [10]. The fact that the result of Ghosal *et al.* [10] is also a special solution of the OC under the condition of the identical distribution solution of $C_{\mathrm{S}}^{\aleph}(\mathbf{x},\mathbf{x}_0)$ can be demonstrated as follows. We have observed that the formulation of the OC is not symmetric in terms of $\mathbf{x}_0$ and $\mathbf{y}$. Under the restriction of identical distribution of $C_{\mathrm{S}}^{\aleph}(\mathbf{x},\mathbf{x}_0)$, $\mathscr{E}_{ij}(\mathbf{x}_0,\mathbf{x}_0)$ can then be reduced to $E_{ij}(\mathbf{x}_0)$ and the OC becomes integrable in terms of $\mathbf{x}_0$, and we obtain

$$\int_{-\infty}^{\infty}E_{ij}(\mathbf{x}_0)\alpha_{ij}(\mathbf{y})\delta_{\mathrm{D}}(\mathbf{x}_0,\mathbf{y})\,\mathrm{d}\mathbf{x}_0-\int_{-\infty}^{\infty}E_{ij}(\mathbf{x}_0)\beta_{ij}(\mathbf{y})G(\mathbf{x}_0,\mathbf{y})\,\mathrm{d}\mathbf{x}_0=0 \tag{47}$$

which can be further rearranged into Equation (19), the result of Ghosal *et al.* [10] as discussed in the previous section. Considering the definition of E_{ij}, i.e. Equation (11), we observe that Equation (19) has one extra integral operation compared with the proposed Equations (43) and (44). Thus, the new PIE proposed in Section 3.2, would be less costly in computation than the conventional FIE2 of Ghosal *et al.* [10]. The above demonstration of the theoretical derivatives of the OC is briefly summarized in Figure 1.

4. PRELIMINARY NUMERICAL APPLICATIONS OF THE OC

In the previous theoretical application of the OC, we obtained three theoretical derivatives, i.e. the DM of Lilly [2], the FIE2 proposed by Ghosal *et al.* [10], and the new DM in the form of a PIE. As indicated earlier, the theoretical potential and applications of the OC are not limited to these three special derivatives. The FIE2 was originally obtained by minimizing a globally integrated residual functional [10]. In spite of its important theoretical value, the FIE2

has only been applied to several cases [10, 16, 37] in the past 10 years due to its complex convolution structure and costly numerical algorithm to solve the integral system. The DM on the other hand, has been relatively widely tested since its invention in 1991 [1, 2, 11, 18, 22], however, it has been confirmed that a plane averaging is often necessary to maintain numerical stability for simulations based on the DM for flows such as pressure- and shear-driven channel flows. Since numerical tests of the conventional DM and FIE2 are not the purpose of this research, we will focus on the numerical validation of the PIE in this study (although the DM of Lilly [2] is used for comparison). It should be noted that the main purpose for presenting the formulation of the PIE in the previous section and its related numerical results in this section, is to demonstrate one possible theoretical and practical application of the OC, the major conclusion of this research. Therefore, in the general structure of this study, theoretical and numerical analyses performed in Sections 3 and 4 are auxiliary to the elucidation of the OC presented previously in Section 2.

The numerical tests were performed using turbulent Couette flow with a physical domain of $L_1 \times L_2 \times L_3 = 8\pi h \times 2h \times 4\pi h$, where h is the half-channel height, set to be 10 mm. Turbulent Couette flow is a canonical test problem for wall-bounded anisotropic turbulence, which has been studied both experimentally [38–43] and numerically [13, 43–49]. The transitional Reynolds number (lowest Reynolds number for which turbulence can be sustained) for Couette flow is $Re_T \approx 600$ according to Leutheusser and Chu [39], while $Re_T \approx 720$ (or $Re_{\tau T} \approx 26$) according to other studies [42–45]. The two Reynolds numbers mentioned above are defined as $Re = U_h(2h)/\nu$ and $Re_\tau = u_\tau h/\nu$. Here, U_h is one half of the velocity difference between the two plates, u_τ is the friction velocity defined as $u_\tau = (\tau_w/\rho)^{1/2}$, and τ_w represents the wall shear stress. The critical Reynolds number for fully developed turbulent Couette flow [43] is $Re_F \approx 1000$ or $Re_{\tau F} \approx 35$. It should be noted that although pressure-driven Poiseuille channel flow has exactly the same physical geometry as shear-driven Couette channel flow, its transitional Reynolds number for turbulence to be sustained and critical Reynolds number for fully developed turbulence are much higher. For pressure-driven channel flows, Patel and Head [50] found the transitional Reynolds number at which a log law with universal constants can be observed is about $Re_{\tau T} \approx 104$; while according to Eckelmann [51], Kim *et al.* [52], and Jiménez and Moin [53], the critical Reynolds number for fully developed flow is $Re_{\tau F} \approx 142$. Thus, both the transitional and critical Reynolds numbers in pressure-driven channel flow are about four times larger than those for shear-driven Couette flow ($104/26 \approx 142/35 \approx 4$).

The fractional step method [54] and second order Adams–Bashforth scheme have been used to discretize the Navier–Stokes equation. A collocated grid system is used in the simulation, and a momentum interpolation scheme for the face flux is adopted to achieve numerical stability for a collocated grid arrangement [55]. Periodic boundary conditions are applied in the streamwise ($\mathbf{x}_1$) and spanwise ($\mathbf{x}_3$) directions, while the no-slip boundary condition is applied in the wall-normal direction ($\mathbf{x}_2$). Statistics for the time averaged quantities are based on 5000 time steps. In the simulations being reported, the Reynolds number ranges from 1500 to 7050 (from $2.1Re_T$ to $9.8Re_T$). For the purpose of comparison, analysis will be focused on the flow patterns for $Re = 2600$, 4762 and 7050, for which data have been documented in the literature. To resolve the turbulence field for $Re = 2600$, Bech *et al.* [43] used $256 \times 70 \times 256$ nodes (non-uniform in the wall-normal direction) in DNS for a field domain of $10\pi h \times 2h \times 4\pi h$, while Kim and Menon [13] used $48 \times 48 \times 32$ nodes (non-uniform in the wall-normal direction) in LES for a field domain of $4\pi h \times 2h \times 2\pi h$. In this study, a coarse uniform grid system of 66^3 control volumes in total was used for all Reynolds numbers. In addition, for the case

of $Re = 2600$, two other uniform grid systems, i.e. 34^3 and 48^3 were also used to examine the grid effect in the simulation.

4.1. Solver for the PIE

In the following context, an efficient implicit solver will be introduced, which makes use of the discrete Gaussian filter and is specific to turbulence with 2-D homogeneity such as pressure-driven Poiseuille channel flow, shear-driven Couette channel flow, flow passing over a flat plate, etc. Sagaut and Grohens [56] reported a useful second order accurate discrete Gaussian filter for LES, i.e.

$$\tilde{\phi}(I,J,K) = \frac{1}{3}\sum_{q=-1}^{1} a_q[\phi(I+q,J,K) + \phi(I,J+q,K) + \phi(I,J,K+q)] \tag{48}$$

where $a_{-1} = a_1 = \frac{1}{24}\varepsilon^2$ and $a_0 = \frac{1}{12}(12 - \varepsilon^2)$. Here, $\varepsilon = \tilde{\bar{\Delta}}/\bar{\Delta}$ represents the ratio of the cut-off filter sizes of the test-grid level and the grid level filters in a dynamic SGS modelling approach. An advantage of choosing the specific value $\varepsilon = 2$ is that the discrete Gaussian filters of the second and fourth orders introduced by Sagaut and Grohens [56] share the same formulation. By substituting the above equation into Equation (43) and averaging the result in the homogeneous plane, the following discrete system can be obtained:

$$\left\{\langle \alpha_{mn} M_{mn}\rangle_p - \frac{a_0}{3}\langle M_{mn}\beta_{mn}\rangle_p - \frac{1}{3}\sum_{q=-1}^{1} a_q\left[\langle M_{mn}\beta_{mn}^{I+q,J,K}\rangle_p + \langle M_{mn}\beta_{mn}^{I,J,K+q}\rangle_p\right]\right\} C_S^J$$
$$-\frac{a_{-1}}{3}\langle M_{mn}\beta_{mn}^{I,J-1,K}\rangle_p C_S^{J-1} - \frac{a_1}{3}\langle M_{mn}\beta_{mn}^{I,J+1,K}\rangle_p C_S^{J+1} + \langle M_{mn}\mathscr{L}_{mn}^*\rangle_p = 0 \tag{49}$$

where $\langle\cdot\rangle_p = \int\int \mathrm{d}x_1\,\mathrm{d}x_3$ represents the planar integral operation, and C_S^J is the model coefficient for the Jth homogeneous plane. The above equation is a 1-D tri-diagonal banded linear system for C_S^J, i.e.

$$\sum_{q=-1}^{1} A_q^J C_S^{J+q} + S^J = 0 \tag{50}$$

which can be readily solved using the conventional tri-diagonal matrix algorithm (TDMA). Here, A_q^J and S^J represent the coefficients and source term contained in Equation (49). The boundary condition is set as $C_S = 0$ at the wall. From a physical point of view, C_S influences the magnitude of the SGS viscosity which is defined as

$$\nu_{sgs} = C_S\bar{\Delta}^2|\bar{S}| \tag{51}$$

Therefore, this boundary condition is compatible with the notion that the SGS stresses vanish at the wall due to the no-slip boundary condition. Since the computational cost of the TDMA is trivial, the above-proposed implicit solver is expected to give both high efficiency and accuracy without any significant additional increase in computational cost. As indicated by Carati *et al.* [16], the relative computational cost for different DMs is difficult to quantify in a precise manner due to its dependence on the computer configuration and details of the code. Nevertheless, we compared the relative computational cost among the proposed PIE, the

Table I. Absolute and relative computational cost ($Re = 2600$).

Grid	66^3		48^3		34^3	
Cost	T/TS (s)	Ratio	T/TS (s)	Ratio	T/TS (s)	Ratio
PIE	43.1	1.04	16.0	1.03	4.4	1.02
DM	41.5	1	15.6	1	4.3	1
SM	22.5	0.54	8.7	0.56	2.7	0.63

standard DM of Lilly [2] and the conventional constant-parameter SM [57]. The comparative study was performed with the same code structure, and the same initial velocity and pressure fields. The cost was measured using the averaged computer time for each time step (T/TS) relative to that of the DM. An ALC PC (Pentium IV-2.66 GHz) was used for evaluating the relative cost. Table I indicates that the T/TS for the SM is only about 54–63% that of the standard DM, while the proposed PIE generally costs only 2–4% more in terms of T/TS than the standard DM, indicating that the additional cost is negligible. In fact, according to our previous research [37], for turbulence with 2-D homogeneous dimensions, even Ghosal's FIE2 can also be solved very efficiently (with an additional cost of about 5% compared to the DM) by applying a similar discretization methodology. It should be noted that although the proposed implicit solver for the PIE and that for the FIE2 [37] have an advantage of being highly efficient, it sacrifices the property that the coefficient should be local not only in the wall-normal direction but also in the homogeneous plane. As we know, both the PIE and FIE2 hold locally at any physical location. Therefore, the computational cost for direct solution of these integral systems for a flow field with complex geometries or without 2-D homogeneity is expected to be much higher. General effective numerical algorithms for locally solving the integral equations of both the PIE and FIE2 [10] need to be pursued in future studies.

4.2. *Basic flow features and discussion*

In this subsection, the features of turbulent Couette flow predicted by the LES using the proposed PIE will be presented. Figure 2 shows the dimensionless velocity profiles obtained for the three Reynolds numbers of 2600, 4762 and 7050. Although the differences in the velocity profiles for the Reynolds number of $Re = 2600$ are very small, the LES result is closer to the DNS result of Bech *et al.* [43] than the experimental data of Aydin and Leutheusser [40]. As expected, the velocity profile at $Re = 7050$ has a narrower wall region than those at $Re = 4762$ and $Re = 2600$. The simulation data of Figure 2 are replotted in Figure 3 using wall coordinates. The prediction for the near-wall velocity profile generally agrees with the experimental results of Robertson and Johnson [38], Bech *et al.* [43], Aydin and Leutheusser [41], as well as the classical two layer wall law [58] given by

$$\begin{aligned} u^+ &= x_2^+ \quad (x_2^+ \leqslant 5) \\ u^+ &= 2.5 \ln(x_2^+) + 5.5 \quad (x_2^+ > 30) \end{aligned} \tag{52}$$

where $u^+ = \langle \bar{u}_1 \rangle / u_\tau$ and $x_2^+ = x_2 u_\tau / \nu$, and $\langle \cdot \rangle$ represents the plane and time averaging operation.

Figures 4(a)–(c) illustrate the wall-normal distributions of the three resolved turbulence intensity components for three different Reynolds numbers, respectively. In Figures 4(a)–(c),

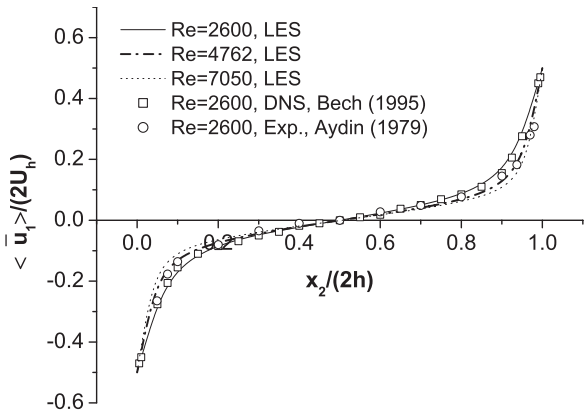

Figure 2. Mean dimensionless velocity profile (66^3 nodes).

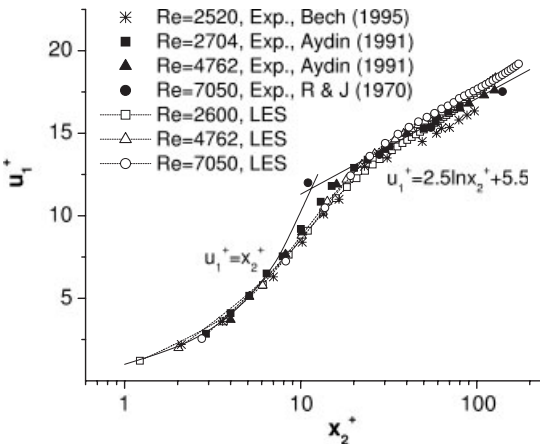

Figure 3. Mean velocity profile in wall coordinates (66^3 nodes).

the residual velocity component is defined as $\bar{u}_i'' = \bar{u}_i - \langle \bar{u}_i \rangle$. As shown in the figures, the peak value for $\langle \bar{u}_1''^2 \rangle^{1/2}/u_\tau$ appears at $x_2^+ = 13$ for $Re = 2600$, $x_2^+ = 15$ for $Re = 4762$ and $x_2^+ = 16$ for $Re = 7050$. These agree approximately with the locations $x_2^+ = 12$ for $Re = 2600$ reported by Bech *et al.* [43], $x_2^+ = 11 \sim 16$ for $Re = 2600$ and 4762 reported by Aydin and Leutheusser [41], and $x_2^+ \approx 16$ for $Re = 7050$ reported by Robertson and Johnson [38]. Figure 4 also indicates that the magnitudes of the peak values of the spanwise and wall-normal components of the turbulence intensities predicted using the PIE are somewhat lower than the DNS results ($Re = 2600$) of Bech *et al.* [43], while the streamwise component is slightly higher than those of the DNS and experimental results. Such a feature that the predicted streamwise turbulence intensity is slightly higher than those predicted by the DNS and measured in experimental studies is characteristic to a coarse grid LES computation, and is consistent with other reported results [3, 59, 60].

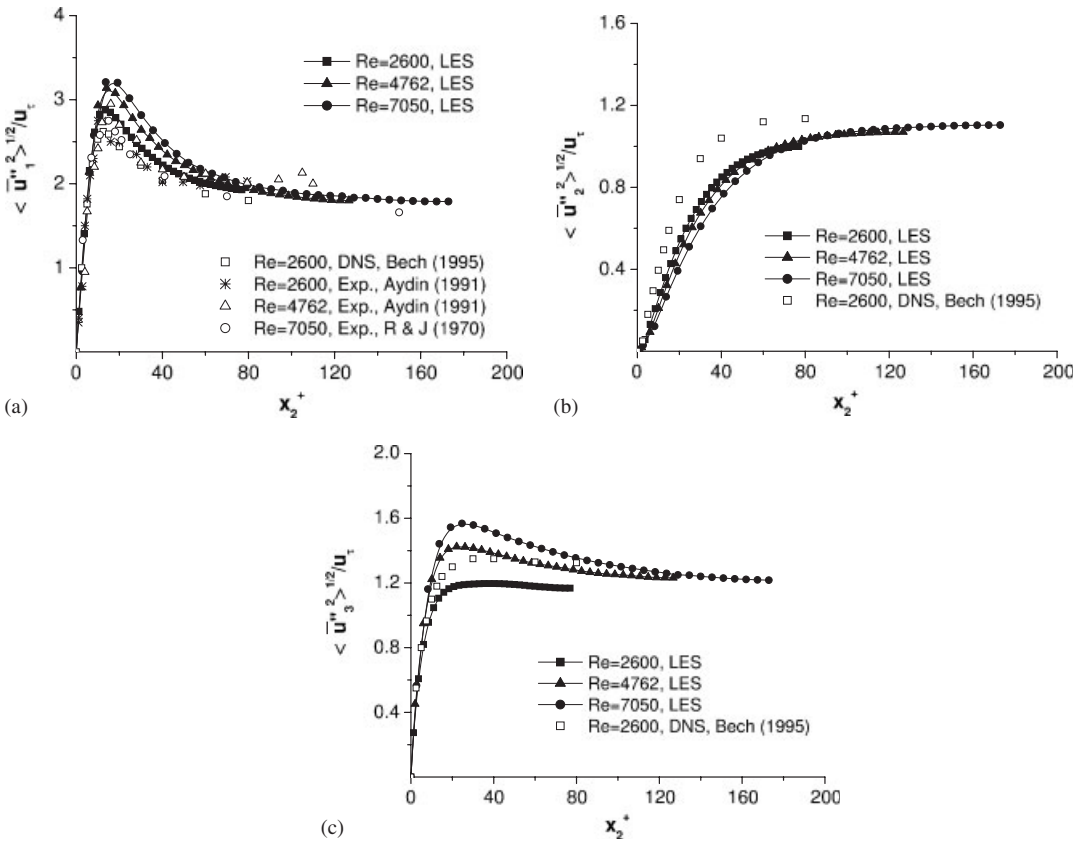

Figure 4. Wall-normal distribution of resolved turbulence intensities (66^3 nodes).

Plane turbulent Couette flow has the unique feature of a constant shear stress distribution, i.e.

$$\mu\langle\bar{u}_{1,2}\rangle - \rho\langle\bar{u}_1''\bar{u}_2\rangle - \rho\langle\tau_{12}\rangle \approx \tau_w = \rho u_\tau^2 \tag{53}$$

The three items on the left-hand side of this equation represent the averaged resolved viscous shear stress, resolved Reynolds shear stress and SGS shear stress, respectively. The above approximate equation was obtained from the filtered streamwise momentum equation based on several assumptions: the flow is steady and homogeneous in the x_1–x_3 plane, and the mean resolved and SGS velocities normal to the homogeneous plane are zero [61, 62], i.e. $\langle\bar{u}_2\rangle = 0$ and $\langle\bar{u}_2''\rangle = 0$. It has been shown both theoretically [63] and numerically [52] that the Reynolds shear stress varies in a cubic manner in the near-wall region. Analysis of the cubic behaviour of the resolved Reynolds shear stress for the (dynamic) Smagorinsky-type SGS models can be found in the works by Piomelli [18, 64] and Pope [65]. As expected, in Figure 5, the resolved Reynolds stress diminishes in the vicinity of the wall following the cubic law, i.e. $-\langle\bar{u}_1''\bar{u}_2\rangle \propto x_2^{+3}$ for $0 \leqslant x_2^+ < 8$.

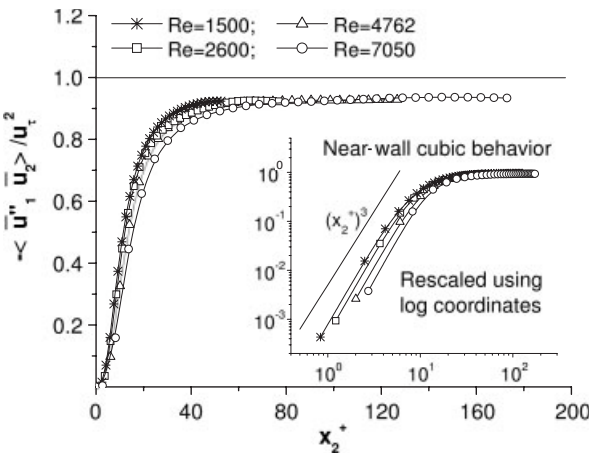

Figure 5. Wall-normal profile of resolved Reynolds shear stress (66^3 nodes).

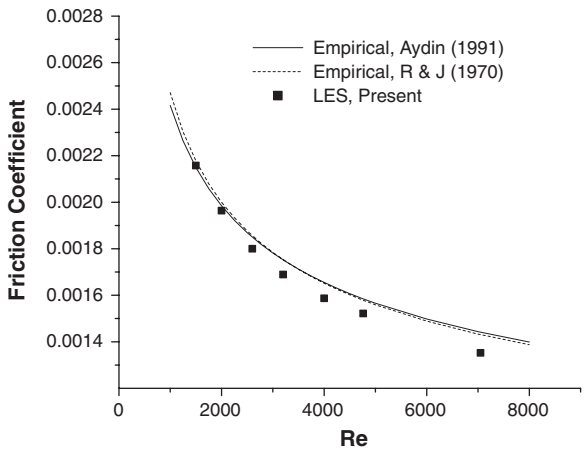

Figure 6. Variation of the skin-friction coefficient C_f with Reynolds number (66^3 nodes).

Figure 6 compares the predicted values of the resolved skin-friction coefficient with the two following empirical friction laws for turbulent Couette flow:

(1) Robertson and Johnson [38]

$$C_f = \frac{0.072}{4[\log(2Re)]^2} \tag{54}$$

(2) Aydin and Leutheusser [41]

$$C_f^{-1/2} = 3.54 \ln(2\, Re\, C_f^{1/2}) + 4.1 \tag{55}$$

where C_f, the friction coefficient, is defined as

$$C_f = \tau_w/(\rho U_0^2/2) = (u_\tau/U_h)^2/2 \tag{56}$$

and $U_0 = 2U_h$ is the velocity difference between the two plates. Figure 6 shows that the resolved friction coefficient obtained from the LES generally agrees with both Equations (54) and (55). Since the near-wall velocity field is less resolved as the Reynolds number increases for a given grid system (66^3 nodes in this case), the resolved velocity gradient component $\bar{u}_{1,2}$ and the consequent wall shear stress τ_w can become underpredicted. Therefore, as expected, the resolved friction coefficient tends to have a lower value than the empirical ones (with a deviation of approximately 8%) at the higher Reynolds numbers.

4.3. Rate of SGS TKE production, norm of filtered strain rate tensor, model coefficient, and SGS viscosity

In order to understand the characteristics of the model coefficient C_S and SGS viscosity ν_{sgs}, we need first to discuss the rate of TKE production for SGS motions $\mathscr{P}_r$, the resolved viscous dissipation rate ε_r, and the norm of the filtered strain rate tensor $|\bar{S}|$. In the following discussion, the results obtained using the 'standard' DM of Lilly [2] are used for comparison to those predicted using the PIE. The *rate of TKE production for SGS motions* $\mathscr{P}_r$ is defined as [65]

$$\mathscr{P}_r = -\tau_{ij}^* \bar{S}_{ij} \tag{57}$$

Following Pope [65], $\mathscr{P}_r$ is referred to as the rate of TKE production for SGS motions instead of the rate of SGS TKE dissipation, since it is analogous to the classical definition of the production term due to the deviatoric part of the Reynolds stress tensor in the RANS (Reynolds Average Navier–Stokes method) approach. Also, $\mathscr{P}_r$ determines the rate of TKE transport from the filtered motions to the residual motions through an inviscid process rather than an actual viscous dissipative process. It acts as a sink of TKE for the filtered-scale motions and as a source of TKE for the residual SGS motions. The *resolved viscous dissipation rate* directly from the filtered field is given by

$$\varepsilon_r = 2\nu \bar{S}_{ij}\bar{S}_{ij} = \nu|\bar{S}|^2 \tag{58}$$

which indicates that $\varepsilon_r \propto |\bar{S}|^2$, i.e. ε_r is an indicator[§] for the magnitude of the filtered strain rate tensor $|\bar{S}|$. Although both $\mathscr{P}_r$ and ε_r represent sinks for TKE of the filtered-scale motions, their mechanisms are entirely different: ε_r is a real dissipation attributed to the resolved viscous effects, while $\mathscr{P}_r$ is due to an inviscid and inertial mechanism, and can also be negative in the case of backscatter.

Figure 7 shows the mean distribution of $\mathscr{P}_r$ along the wall-normal direction in terms of both dimensional and nondimensional values. It is observed that the $\mathscr{P}_r$ profiles predicted using both the DM and PIE, exhibit a general anisotropy due to the restriction by the wall:

[§]Let $\langle x \rangle$ represent an averaged result, i.e. $\langle x \rangle = (1/N)\sum_{i=1}^{N} x_i$. From statistics, we know that, *in general*, $\langle xy \rangle \neq \langle x \rangle \langle y \rangle$. Thus, for $Pr = \nu_{sgs}|\bar{S}|^2$ we have $\langle Pr \rangle = \langle \nu_{sgs}|\bar{S}|^2 \rangle \neq \langle \nu_{sgs} \rangle \langle |\bar{S}| \rangle \langle |\bar{S}| \rangle$; and for $\varepsilon_r = \nu|\bar{S}|^2$, we have $\langle \varepsilon_r \rangle = \nu\langle |\bar{S}|^2 \rangle \neq \nu \langle |\bar{S}| \rangle \langle |\bar{S}| \rangle$. Strictly speaking, although the averaged value of $\langle Pr \rangle$, $\langle \varepsilon_r \rangle$ and $\langle \nu_{sgs} \rangle$ are known, $\langle |\bar{S}| \rangle$ cannot be directly inferred from these values.

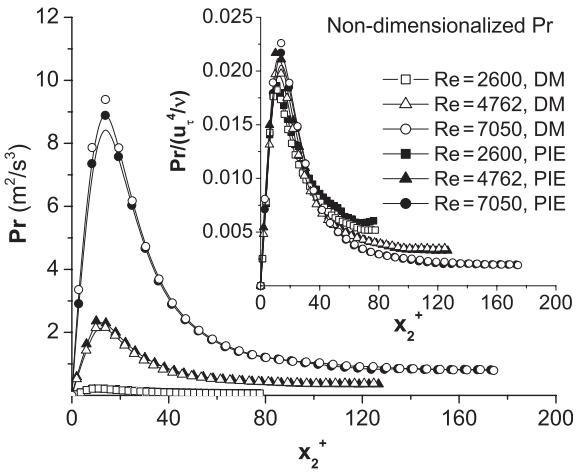

Figure 7. Averaged rate of TKE production for SGS motions in the wall-normal direction (66^3 nodes).

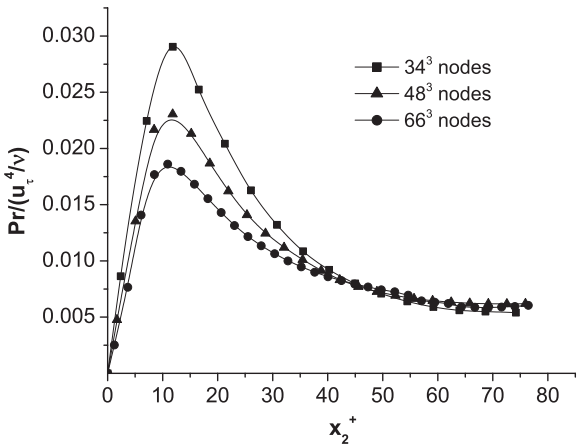

Figure 8. Grid effect on the rate of TKE production for SGS motions ($Re = 2600$).

it is lower in the central region and peaks in the near-wall region around $x_2^+ = 13$. From the dimensional diagram, it is observed that the profile of $\mathscr{P}_r$ is sensitive to the Reynolds number, i.e. the absolute value of $\mathscr{P}_r$ increases dramatically as the Reynolds number increases. This is explained by the fact that for the same discrete grid system, a higher Reynolds number turbulent flow has 'more' net TKE to be transferred from the resolved to SGS motions. Figure 8 demonstrates the grid effect on the $\mathscr{P}_r$ term. Clearly, as the grid becomes coarser, the nondimensional value of $\mathscr{P}_r$ increases in the boundary layer region, especially around the peak location.

Equation (57) is a general definition for $\mathscr{P}_r$, which is applicable to any SGS constitutive relations. In general, e.g. for the dynamic two-parameter mixed models [20, 21, 29, 62, 66, 67]

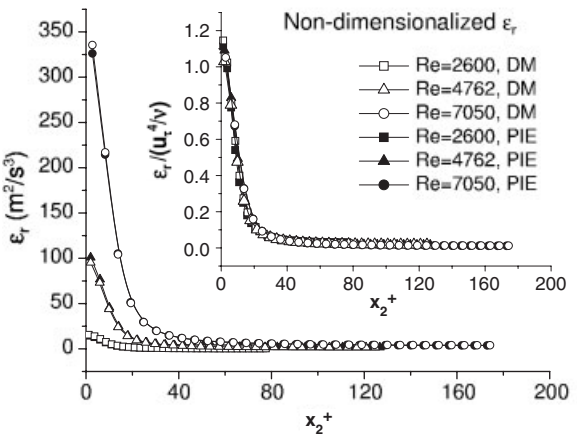

Figure 9. Resolved viscous dissipation in the wall-normal direction (66^3 nodes).

and the nonlinear quadratic DMs [3, 4, 23, 24], the value of $\mathscr{P}_r$ is decided by both the magnitudes of $-\tau_{ij}$ and $\bar{S}_{ij}$, as well as their relative tensorial geometrical relation. The importance of the tensorial geometry of the negative SGS stress and filtered strain rate tensors has lately been indicated by several studies based on *a priori* approaches [68–70] and *a posteriori* approaches [3, 4, 71, 72]. Since the three principal axes (orthonormal eigenvectors) of $-\tau_{ij}$ are not necessarily aligned with those of $\bar{S}_{ij}$ in the general case, various possibilities exist, one of which is the specific theoretical situation that an instantaneous orthogonality is allowed to exist between the $-\tau_{ij}$ and $\bar{S}_{ij}$ such that their production is trivial, i.e. $\mathscr{P}_r = -\tau_{ij}^* \bar{S}_{ij} = 0$ (although the value of $\|\tau_{ij}\|$ and $|\bar{S}|$ may still be very large). For the Smagorinsky-type models, the case that $\mathscr{P}_r = 0$ due to such an orthogonality never exists, since the principal axes of $-\tau_{ij}$ are always aligned with those of $\bar{S}_{ij}$. Furthermore, for the Smagorinsky-type models, if $\mathscr{P}_r = 0$ and $\bar{\Delta} \neq 0$ then at least one of the two following conditions must be true: $C_S = 0$ and/or $|\bar{S}| = 0$. Thus, in general, a higher $\mathscr{P}_r$ is not a sufficient condition for a larger value of C_S or v_{sgs}, because the value of $\mathscr{P}_r$ is determined not only by the relative tensorial magnitudes of $-\tau_{ij}$ and $\bar{S}_{ij}$ but also by the relative geometry between them as well. Notwithstanding the general case, in the particular case of the Smagorinsky-type models, $\mathscr{P}_r$ takes the following form on substituting Equation (3):

$$\mathscr{P}_r = v_{sgs}|\bar{S}|^2 = C_S \bar{\Delta}^2 |\bar{S}|^3 \tag{59}$$

Thus, for a particular turbulent flow with the Reynolds number specified, $\mathscr{P}_r = \mathscr{P}_r(v_{sgs}, |\bar{S}|) = \mathscr{P}_r(C_S, \bar{\Delta}, |\bar{S}|)$ when a Smagorinsky constitutive relation is adopted for the SGS model. From previous analysis, we understand that a higher Reynolds number corresponds to a higher level of $\mathscr{P}_r$. While from Equation (59), it is understood that a higher level of $\mathscr{P}_r$ does not necessarily correspond to larger values of C_S or v_{sgs}, because the norm of the filtered strain $|\bar{S}|$ is also involved which responds to the Reynolds number independently.

Figures 9 and 10 plot the dimensional and nondimensional profiles of the resolved viscous dissipation rate ε_r in the wall-normal direction for the entire channel and the core region.

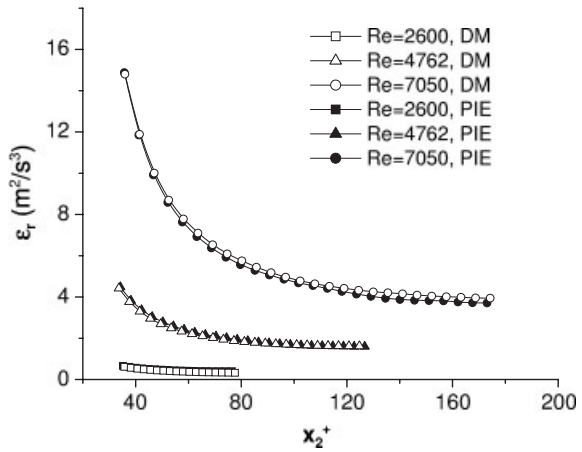

Figure 10. Resolved viscous dissipation rate in the core region (66^3 nodes).

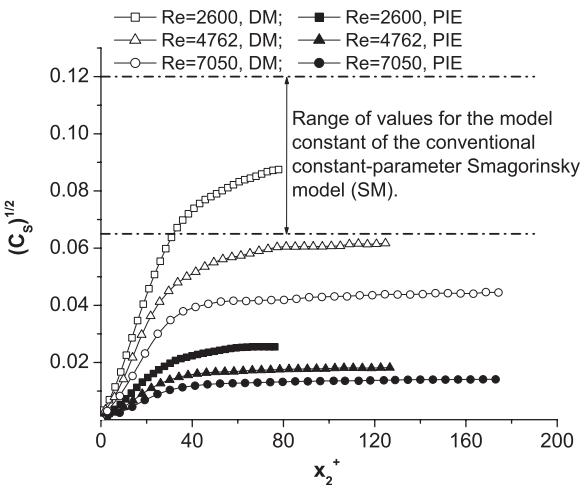

Figure 11. Mean distribution of model coefficient in the wall-normal direction (66^3 nodes).

From the dimensional profiles, it is observed that both ε_r and $|\bar{S}|$ increase with the Reynolds number. As shown in both the dimensional and non-dimensional diagrams, ε_r increases drastically as the wall is approached especially within $x_2^+ < 30$. This indicates a strong anisotropic distribution of the norm of the filtered strain rate tensor $|\bar{S}|$ along the wall-normal direction. The near-wall anisotropy of $|\bar{S}|$ is due to the behaviour of the dominant velocity gradient component $\bar{u}_{1,2}$, whose value changes drastically in the near-wall region and in an average sense reaches a maximum at the wall.

Figure 11 illustrates the mean distribution of the proposed model coefficient C_S along the wall-normal direction in comparison with those calculated using the conventional DM [2] and SM [57]. In Figure 11, $C_S^{1/2}$ instead of C_S is used because the conventional SM

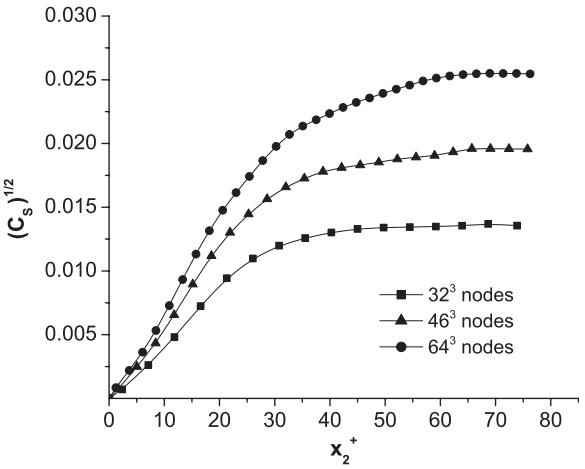

Figure 12. Grid effect on model coefficient ($Re = 2600$).

[57] uses C_S^2 (instead of C_S) to model the SGS stress tensor in Equation (3). As shown in Figure 11, the value of the Smagorinsky constant for the SM typically [19, 34, 64] ranges from 0.065 to 0.12, however, the value of $C_S^{1/2}$ for the PIE ranges only from 0.014 ($Re = 7050$) to 0.026 ($Re = 2600$) in the core region. The model coefficient profile for both the DM and PIE vanishes at the wall, which is due to the requirement that the SGS viscosity must vanish at the wall ($v_{sgs}|_{x_2^+=0} \equiv 0$). This is intrinsically different than the approach of the conventional SM [57], in which case this near-wall physical requirement is forced to be realized by an *ad hoc* geometric damping function instead of the model itself, for instance [18], $d(x_2^+) = [1 - \exp(-x_2^{+3}/25^3)]$. Also, as demonstrated in Figure 11, for the three Reynolds numbers tested, the value of $C_S^{1/2}$ for the PIE is about 30% that of the DM, although both the DM and PIE are dynamic SGS models based on the same Smagorinsky constitutive relation. Furthermore, it is observed from Figure 11 that as the Reynolds number increases, the value of C_S decreases for both the PIE and DM, which confirms our previous analysis that for the dynamic SM, a higher Reynolds number does not necessarily relate to a larger C_S because of the involvement of $|\tilde{S}|$ which is a function of Re (see Equation (58) and Figures 9 and 10). Figure 12 demonstrates the grid scale effect on the wall-normal distribution of the model coefficient calculated using the PIE. From the figure, two characteristics of the modelling coefficient can be concluded, i.e. C_S is not a grid invariant in a dynamic procedure, which is in sharp contrast to the conventional SM approach [57]; also, a coarser grid does not necessarily warrant a larger value of C_S since it is the SGS viscosity v_{sgs} rather than C_S that plays a more important role in the Smagorinsky types of models. In the next paragraph, we will further clarify the relation between v_{sgs} and C_S.

Figure 13 demonstrates that as the Reynolds number increases, the profile of the SGS viscosity v_{sgs} increases only slightly in the buffer region, which is in contrast to the large change in the C_S profile shown in Figure 11. The explanation lies in the definition of v_{sgs}, which indicates that for any particular instantaneous flow field (Re must be specified), v_{sgs} is a function of the grid level filter size, C_S and $|\tilde{S}|$, i.e. $v_{sgs} = v_{sgs}(\tilde{\Delta}, C_S, |\tilde{S}|)$. Thus, it is clear

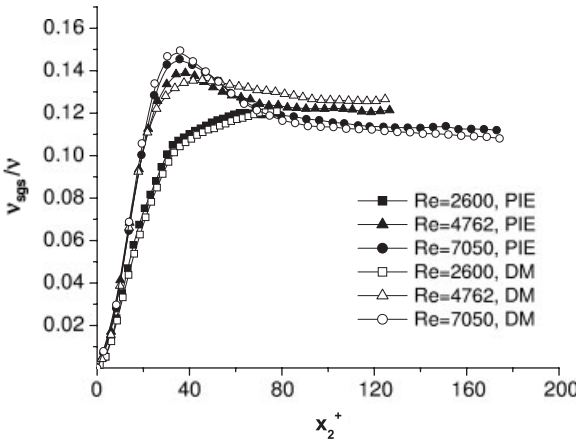

Figure 13. Mean SGS viscosity profile in the wall-normal direction (66^3 nodes).

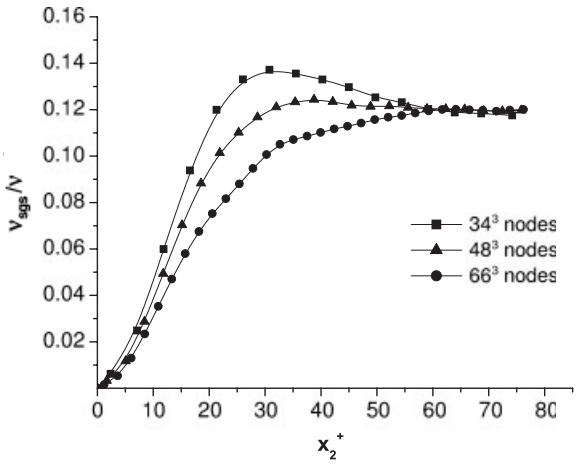

Figure 14. Grid effect on SGS viscosity ($Re = 2600$).

that a larger value of v_{sgs} does not necessarily correspond to a large value of C_S due to the involvement of $|\bar{S}|$ (if $\bar{\Delta}$ is fixed). In fact, from Figures 9 and 10, we understand that $|\bar{S}|$ increases drastically with Re, which explains the difference between the Reynolds number effects on C_S and v_{sgs}. Figure 13 indicates that the buffer region (especially around $x_2^+ \approx 30$) responds to the Reynolds number more actively than other parts of the flow in terms of v_{sgs}. Such an anisotropic behaviour of v_{sgs} is consistent with its definition (Equation (51)) and the near-wall anisotropic effect of $|\bar{S}|$ and C_S as illustrated in Figures 9 and 11, respectively. Figure 14 indicates that the buffer region also responds to the grid scale more sensitively than other regions in terms of the value of v_{sgs}.

Finally, we briefly comment on the non-dimensionalization method for the SGS viscosity used in this research. From the Equations (58) and (59), it is understood that v_{sgs}/v has a special meaning unique for the Smagorinsky constitutive relation: the ratio v_{sgs}/v actually describes the relative magnitudes of the two sinks for the TKE for the filtered motions, i.e. $\mathscr{P}_r/\varepsilon_r \equiv v_{sgs}/v$.

5. CONCLUSIONS

This paper provides a consistent mathematical treatment for the local optimal dynamic Smagorinsky SGS stress model, as well as revisits the Smagorinsky relation from the point of functional variation and function approximation. In contrast to the previous approaches [10, 16], the local error density functional $\mathscr{Q}$ has been successfully minimized in a direct manner without resorting to a global integration. The properties of the variations of the local error functional at different orders have been examined, and the possibilities of the non-extremum inflection and saddle points have been strictly excluded from the solution set of the local error functional minimization. A sufficient and necessary condition for local optimization of the dynamic Smagorinsky model using functional variational theory has been obtained, which is in the form of an orthogonal condition (OC) and controls the local optimal model coefficient for a dynamic Smagorinsky SGS model. The OC is a useful tool in dynamic SGS modelling optimization, which unifies a few conventional modelling formulations as its special theoretical solutions under difference restrictions. These conventional formulations include the dynamic model (DM) of Germano *et al.* [1] and Lilly [2], and the Fredholm integral equation of the second kind (FIE2) of Ghosal *et al.* [10].

From the integral form of the OC, a Fredholm integral equation of the third kind or Picard's integral equation (PIE) has been derived, which is necessary to make the local error density $\mathscr{Q}$ minimum. Similar to the FIE2 [10], this PIE holds locally at any point and needs to be solved only once for the entire domain. The proposed PIE has one less convolution operation than the FIE2 of Ghosal *et al.* [10], and therefore it is less expensive to compute. It should be noted that as the sufficient and necessary condition for localization, the OC implies other theoretical applications, and the PIE is only one of its derivatives.

For the purpose of demonstrating the theoretical potential of the OC as well as the possibility of applying it in practice, numerical tests based on the PIE have been performed using turbulent Couette flow. Some salient features of this prototypical near-wall turbulent flow have been obtained based on comparisons with the experimental and DNS results of other researchers. These features include the existence of a logarithmic mean velocity profile, the characteristic anisotropic wall-normal distribution of the turbulent intensities, and a near-wall cubic behaviour for the resolved Reynolds shear stress. In order to solve the PIE effectively, an implicit solution scheme with an additional computational cost of less than 4% compared to the DM, has been developed by using the discrete Gaussian filter of Sagaut and Grohens [56]. It should be noted that this efficient implicit solution scheme for the PIE holds when it is acceptable to assume 2-D homogeneity in a flow field. However, the computational cost for direct solution of these integral systems for a flow field with complex geometries or without 2-D homogeneity is expected to be much higher, and general effective numerical algorithms for solving the integral equation of the PIE locally need to be pursued in future studies.

Physical meanings for such grid and test-grid level tensors as α_{ij}, β_{ij}, M_{ij}, M'_{ij}, $\mathscr{L}_{ij}^{\text{appr}^*}$ and $\mathscr{L}_{ij}^{\text{proj}^*}$ have been proposed by identifying their role in various constitutive and constructive relations. The construction of the approximation tensor space for the projection of the Leonard stress has also been investigated, including the approximation tensor space of Lilly's original approach $\mathfrak{M}_{\text{L}}^{\text{orig}}$ [2], that of the revised approach of Lilly $\mathfrak{M}_{\text{L}}^{\text{rev}}$, and that of the general local optimization approach $\mathfrak{M}_{\text{o}}$. These approximation tensor spaces for the Leonard stress are essential to the optimization methods adopted for deriving the dynamic localization models using the local minimal residual of the Germano identity as the criterion.

For the Smagorinsky constitutive relation, the norm of the filtered strain rate tensor $|\bar{S}|$ is found to play a key role in determining the relative magnitudes of the SGS stress τ_{ij}, rate of TKE production for SGS motions $\mathscr{P}_r$, SGS viscosity ν_{sgs}, and model coefficient C_{S}. The value of $|\bar{S}|$ (indicated by the resolved viscous dissipation rate ε_r) changes dramatically with the Reynolds number, especially within the near-wall region for $x_2^+ < 30$. Given that all the other test conditions are the same, the mean rate of TKE production for SGS motions $\mathscr{P}_r$ increases as the Reynolds number increases, indicating a more massive net transfer of TKE between the filtered and subgrid scales of motions. From the definition of the SGS viscosity, it is understood that a large value of ν_{sgs} does not of itself require a large value of C_{S} because of the involvement of $|\bar{S}|$. For a specific flow (with the grid level filter and *Re* specified), $\mathscr{P}_r$ changes with C_{S} and $|\bar{S}|^3$, or with ν_{sgs} and $|\bar{S}|^2$, and therefore due to the involvement of $|\bar{S}|$, a higher level of $\mathscr{P}_r$ is not a sufficient condition for a higher level of C_{S} or ν_{sgs}.

In general, this research attempts to investigate the properties of the local optimal SGS stress model *strictly within* the framework of the classical Smagorinsky constitutive relation. It is not intended for claiming the 'best' model or evaluating different optimal SGS stress models without a restriction of the constitutive relations. An engagement of this systematic study of the Smagorinsky-type optimal models does not imply that the authors view the Smagorinsky-type models as the best approach for LES. Instead, it should be indicated that many drawbacks of the (dynamic) Smagorinsky models originate from the simplicity of its assumed linear Boussinesq constitutive relation. An increasing body of research [3, 4, 7, 23, 24, 68] suggests that instead of performing optimization for the dynamic procedure within the simple Smagorinsky constitutive framework, which usually results in a formulation that is relatively difficult to solve (e.g. an integral equation), improved methods may consider non-Smagorinsky constitutive relations in the dynamic modelling procedure [3, 4, 7, 20, 21, 23, 24, 29, 62, 66, 67]. Nevertheless, an extensive discussion of this topic is still very useful, because so far the (dynamic) Smagorinsky-type models are still the most popular in the LES community.

APPENDIX A: PROOF OF SUFFICIENCY

In Section 2, the OC has been proven necessary for minimizing the local error functional $\mathscr{Q}$. In this appendix, we further give the proof that the OC is also a sufficient condition.

Solutions obtained from the variational condition (Equation (24)) or the OC (Equation (28)), can be extremum functions, or non-extremum inflection or saddle 'points' (functions actually) for the local error functional $\mathscr{Q}(C_{\text{S}}(\mathbf{x}_0, \mathbf{x}_0))$. To investigate the sufficient condition for the minimal $\mathscr{Q}$, its second and higher order variations must be considered. Assuming that $\mathscr{Q}[C_{\text{S}}(\mathbf{x}_0, \mathbf{x}_0) + \eta\delta C_{\text{S}}(\mathbf{x}_0, \mathbf{x}_0)]$ is at least three times differentiable with respect

to η, where η is all sufficiently small numbers near 0, then the following results for the second and nth order variations can be readily obtained from their definitions [35]:

$$\delta^2 \mathscr{Q}(C_S(\mathbf{x}_0,\mathbf{x}_0),\eta\delta C_S(\mathbf{x}_0,\mathbf{x}_0)) = \frac{d^2}{d\eta^2}\mathscr{Q}(C_S(\mathbf{x}_0,\mathbf{x}_0)+\eta\delta C_S(\mathbf{x}_0,\mathbf{x}_0))\Big|_{\eta=0}$$
$$= 2\delta\mathscr{E}_{ij}\delta\mathscr{E}_{ij} \geqslant 0 \tag{A1}$$
$$\delta^n \mathscr{Q}(C_S(\mathbf{x}_0,\mathbf{x}_0),\eta\delta C_S(\mathbf{x}_0,\mathbf{x}_0)) = \frac{d^n}{d\eta^n}\mathscr{Q}[C_S(\mathbf{x}_0,\mathbf{x}_0)+\eta\delta C_S(\mathbf{x}_0,\mathbf{x}_0)]\Big|_{\eta=0} \equiv 0 \tag{A2}$$

at any given location $\mathbf{x}_0$ and for $n \geqslant 3$.

Suppose that the function $C_S^{\aleph}(\mathbf{x},\mathbf{x}_0)$ is a solution of the OC, which makes the first order variation of $\mathscr{Q}$ vanish. The possibility for $C_S^{\aleph}(\mathbf{x},\mathbf{x}_0)$ to be an inflection 'point' can be excluded by condition (A1), which does not allow the sign of $\delta^2\mathscr{Q}$ to change at $C_S^{\aleph}(\mathbf{x},\mathbf{x}_0)$. It can be shown that the functional $\mathscr{Q}$ can be expanded using its variations in the following manner [35]:

$$\mathscr{Q}(C_S^{\aleph}(\mathbf{x}_0,\mathbf{x}_0)+\eta\delta C_S(\mathbf{x}_0,\mathbf{x}_0)) = \sum_{n=0}^{3}\frac{\eta^n}{n!}\delta^n\mathscr{Q}(C_S^{\aleph}(\mathbf{x}_0,\mathbf{x}_0),\delta C_S(\mathbf{x}_0,\mathbf{x}_0))$$
$$+R_3(C_S^{\aleph}(\mathbf{x}_0,\mathbf{x}_0),\delta C_S(\mathbf{x}_0,\mathbf{x}_0),\eta) \tag{A3}$$

where $R_3 = R_3(C_S^{\aleph}(\mathbf{x}_0,\mathbf{x}_0),\delta C_S(\mathbf{x}_0,\mathbf{x}_0),\eta)$ is the truncation error, which is restricted by

$$|R_3| \leqslant \frac{|\eta|^3}{3!}\max_{|\sigma|\leqslant|\eta|}\left|\frac{d^3}{d\sigma^3}\mathscr{Q}(C_S^{\aleph}(\mathbf{x}_0,\mathbf{x}_0)+\sigma\delta C_S(\mathbf{x}_0)) - \delta^3\mathscr{Q}(C_S^{\aleph}(\mathbf{x}_0,\mathbf{x}_0),\delta C_S(\mathbf{x}_0,\mathbf{x}_0))\right| \tag{A4}$$

$\forall\,\eta$ and σ near 0. Since the third order derivative and variation vanish as shown in Equation (A2), we know that $|R_3| \equiv 0$. This result can also be understood in the following intuitive way: from Equations (20) and (21), we understand that $\mathscr{Q} = \mathscr{E}_{ij}\mathscr{E}_{ij}$ is a second order functional of $C_S(\mathbf{x},\mathbf{x}_0)$ and thus its third and higher order variations must vanish and $|R_3| \equiv 0$. Considering that the first order variation vanishes, then Equation (A3) can be simplified to

$$\mathscr{Q}(C_S^{\aleph}(\mathbf{x}_0,\mathbf{x}_0)+\eta\delta C_S(\mathbf{x}_0,\mathbf{x}_0)) = \mathscr{Q}(C_S^{\aleph}(\mathbf{x}_0,\mathbf{x}_0)) + \frac{\eta^2}{2!}\delta^2\mathscr{Q}(C_S^{\aleph}(\mathbf{x}_0,\mathbf{x}_0),\delta C_S(\mathbf{x}_0,\mathbf{x}_0)) \tag{A5}$$

Using (A1), we obtain

$$\mathscr{Q}(C_S^{\aleph}(\mathbf{x}_0,\mathbf{x}_0)+\eta\delta C_S(\mathbf{x}_0,\mathbf{x}_0)) \geqslant \mathscr{Q}(C_S^{\aleph}(\mathbf{x}_0,\mathbf{x}_0)) \tag{A6}$$

The above result clearly indicates that at any given location $\mathbf{x}_0$, $C_S^{\aleph}(\mathbf{x},\mathbf{x}_0)$ which satisfies the necessary condition will only allow $\mathscr{Q}$ to be locally minimal. Thus the variational condition and its equivalent expression, i.e. the OC or DEC, are not only necessary but also sufficient for minimizing the local error functional $\mathscr{Q}$. The possibility for $C_S^{\aleph}(\mathbf{x},\mathbf{x}_0)$ to be a saddle point has automatically been excluded, because Equation (A6) prohibits $\left[\mathscr{Q}(C_S^{\aleph}(\mathbf{x}_0,\mathbf{x}_0)+\eta\delta C_S(\mathbf{x}_0,\mathbf{x}_0)) - \mathscr{Q}(C_S^{\aleph}(\mathbf{x}_0,\mathbf{x}_0))\right]$ from changing sign at $C_S^{\aleph}(\mathbf{x},\mathbf{x}_0)$.

ACKNOWLEDGEMENTS

The authors would like to thank Dr Fang-Xiang Wu for many helpful discussions regarding the mathematical analysis. The support of NSERC (Natural Sciences and Engineering Research Council) in the form of a research grant is also gratefully acknowledged.

REFERENCES

1. Germano M, Piomelli U, Moin P, Cabot WH. A dynamic subgrid-scale eddy viscosity model. *Physics of Fluids A* 1991; **3**:1760–1765.
2. Lilly DK. A proposed modification of the Germano subgrid-scale closure method. *Physics of Fluids A* 1992; **4**:633–635.
3. Wang B-C, Bergstrom DJ. A dynamic nonlinear subgrid-scale stress model. *Physics of Fluids* 2005; **17**:(035109)1–15.
4. Wang B-C, Yin J, Yee E, Bergstrom DJ. Turbulence topologies predicted via dynamic nonlinear subgrid-scale model based on Speziale's quadratic constitutive relation. *Proceedings of the 4th International Symposium on Turbulence and Shear Flow Phenomena*, Williamsburg, Virginia, 2005, in press.
5. Lumley JL. Toward a turbulent constitutive relation. *Journal of Fluid Mechanics* 1970; **41**:413–434.
6. Pope SB. A more general effective-viscosity hypothesis. *Journal of Fluid Mechanics* 1975; **72**:331–340.
7. Lund TS, Novikov EA. Parameterization of subgrid-scale stress by the velocity gradient tensor. *Annual Research Briefs*, CTR, Stanford University, 1992; 27–43.
8. Langford JA, Moser RD. Optimal LES formulations for isotropic turbulence. *Journal of Fluid Mechanics* 1999; **398**:321–346.
9. Zandonade PS, Langford JA, Moser RD. Finite-volume optimal large-eddy simulation of isotropic turbulence. *Physics of Fluids* 2004; **16**:2255–2271.
10. Ghosal S, Lund TS, Moin P, Akselvoll K. A dynamic localization model for large-eddy simulation of turbulent flows. *Journal of Fluid Mechanics* 1995; **286**:229–255.
11. Piomelli U, Liu J. Large-eddy simulation of rotating channel flows using a localized dynamic model. *Physics of Fluids* 1995; **7**:839–848.
12. Menon S, Yeung P-K, Kim W-W. Effect of subgrid models on the computed interscale energy transfer in isotropic turbulence. *Computers and Fluids* 1996; **25**:165–180.
13. Kim W-W, Menon S. An unsteady incompressible Navier–Stokes solver for large eddy simulation of turbulent flows. *International Journal for Numerical Methods in Fluids* 1999; **31**:983–1017.
14. Pallares J, Davidson L. Large-eddy simulations of turbulent flow in a rotating square duct. *Physics of Fluids* 2000; **12**:2878–2894.
15. Liu S, Meneveau C, Katz J. On the properties of similarity subgrid-scale models as deduced from measurements in a turbulent jet. *Journal of Fluid Mechanics* 1994; **275**:83–119.
16. Carati D, Ghosal S, Moin P. On the representation of backscatter in dynamic localization models. *Physics of Fluids* 1995; **7**:606–616.
17. Oden JT. *Applied Functional Analysis*: *A First Course for Students of Mechanics and Engineering Science*. Prentice-Hall Press: Englewood Cliffs, NJ, 1979.
18. Piomelli U. High Reynolds number calculations using the dynamic subgrid-scale stress model. *Physics of Fluids A* 1993; **5**:1484–1490.
19. Sagaut P. *Large Eddy Simulation for Incompressible Flows*: *An Introduction* (2nd edn). Springer: Berlin, 2002.
20. Salvetti MV, Banerjee S. *A priori* tests of a new dynamic subgrid-scale model for finite-difference large-eddy simulations. *Physics of Fluids* 1995; **7**:2831–2847.
21. Morinishi Y, Vasilyev OV. A recommended modification to the dynamic two-parameter mixed subgrid scale model for large eddy simulation of wall bounded turbulent flow. *Physics of Fluids* 2001; **13**:3400–3410.
22. Moin P, Squires K, Cabot W, Lee S. A dynamic subgrid-scale model for compressible turbulence and scalar transport. *Physics of Fluids A* 1991; **3**:2746–2757.
23. Wong VC. A proposed statistical-dynamic closure method for the linear and non-linear subgrid-scale stresses. *Physics of Fluids A* 1992; **4**:1080–1082.
24. Kosović B. Subgrid-scale modelling for the large-eddy simulation of high-Reynolds-number boundary layers. *Journal of Fluid Mechanics* 1997; **336**:151–182.
25. Meneveau C, Lund TS, Moin P. Search for subgrid scale parameterization by projection pursuit regression. *Proceedings of the CTR Summer Program*, Stanford University, 1992; 61–81.
26. Kuerten JGM, Geurts BJ, Vreman AW, Germano M. Dynamic inverse modelling and its testing in large-eddy simulations of the mixing layer. *Physics of Fluids* 1999; **11**:3778–3785.
27. Morinishi Y, Vasilyev OV. Vector level identity for dynamic subgrid scale modeling in large eddy simulation. *Physics of Fluids* 2002; **14**:3616–3623.

28. Ronchi C, Ypma M, Canuto VM. On the application of the Germano identity to subgrid-scale modelling. *Physics of Fluids A* 1992; **4**:2927–2929.
29. Meneveau C, Katz J. Dynamic testing of subgrid models in large eddy simulation based on the Germano identity. *Physics of Fluids* 1999; **11**:245–247.
30. Brun C, Friedrich R. Modelling of the test SGS tensor T_{ij}: an issue in the dynamic approach. *Physics of Fluids* 2001; **13**:2373–2385.
31. Kanwal RP. *Generalized Functions*: *Theory and Technique* (2nd edn). Birkhäuser Press: Rensselaer, NY, 1997.
32. Spencer AJM. Theory of invariants. In *Continuum Physics*, Eringen AC (ed.). Academic Press: New York, 1971.
33. Gatski TB, Speziale CG. On explicit algebraic stress models for complex turbulent flows. *Journal of Fluid Mechanics* 1993; **254**:59–78.
34. Canuto VM, Cheng Y. Determination of the Smagorinsky–Lilly constant C_S. *Physics of Fluids* 1997; **9**: 1368–1378.
35. Smith DR. *Variational Methods in Optimization*. Prentice-Hall Press: Englewood Cliffs, NJ, 1974.
36. Kondo J. *Integral Equations*. Oxford Applied Mathematics and Computing Science Series. Oxford University Press: Tokyo, 1991.
37. Wang B-C, Bergstrom DJ. An efficient solution scheme for applying the integral type dynamic localization subgrid-scale model in turbulence with homogeneous directions. *Numerical Heat Transfer*: *Part B* 2004; **45**:201–220.
38. Robertson JM, Johnson HF. Turbulence structure in plane Couette flow. *Journal of the Engineering Mechanics Division* (ASCE) 1970; **96**:1171–1182.
39. Leutheusser HJ, Chu VH. Experiments on plane Couette flow. *Journal of the Hydraulics Division* (ASCE) 1971; **97**:1269–1284.
40. Aydin M, Leutheusser HJ. Novel experimental facility for the study of plane Couette flow. *Review of Scientific Instruments* 1979; **50**:1362–1366.
41. Aydin EM, Leutheusser HJ. Plane-Couette flow between smooth and rough walls. *Experiments in Fluids* 1991; **11**:302–312.
42. Tillmark N, Alfredsson PH. Experiments on transition in plane Couette flow. *Journal of Fluid Mechanics* 1992; **235**:89–102.
43. Bech K, Tillmark N, Alfredsson PH, Andersson HI. An investigation of turbulent plane Couette flow at low Reynolds numbers. *Journal of Fluid Mechanics* 1995; **286**:291–325.
44. Lundbladh A, Johansson AV. Direct simulation of turbulent spots in plane Couette flow. *Journal of Fluid Mechanics* 1991; **229**:499–516.
45. Komminaho J, Lundbladh A, Johansson AV. Very large structures in plane Couette flow. *Journal of Fluid Mechanics* 1996; **320**:259–285.
46. Hamilton JM, Kim J, Waleffe F. Regeneration mechanisms of near-wall turbulence structures. *Journal of Fluid Mechanics* 1995; **287**:317–348.
47. Papavassiliou DV, Hanratty TJ. Interpretation of large-scale structures observed in a turbulent plane Couette flow. *International Journal of Heat and Fluid Flow* 1997; **18**:55–69.
48. Kawahara G, Kinda S. Periodic motion embedded in plane Couette turbulence: regeneration cycle and burst. *Journal of Fluid Mechanics* 2001; **449**:291–300.
49. Komminaho J, Skote M. Reynolds stress budgets in Couette and boundary layer flows. *Flow*, *Turbulence and Combustion* 2002; **68**:167–192.
50. Patel VC, Head MR. Some observations on skin friction and velocity profiles in fully developed pipe and channel flows. *Journal of Fluid Mechanics* 1969; **38**:181–201.
51. Eckelmann H. The structure of the viscous sublayer and the adjacent wall region in a turbulent channel flow. *Journal of Fluid Mechanics* 1974; **65**:439–459.
52. Kim J, Moin P, Moser R. Turbulence statistics in fully developed channel flow at low Reynolds number. *Journal of Fluid Mechanics* 1987; **177**:133–166.
53. Jiménez J, Moin P. The minimal flow unit in near-wall turbulence. *Journal of Fluid Mechanics* 1991; **225**: 213–240.
54. Kim J, Moin P. Application of a fractional-step method to incompressible Navier–Stokes equations. *Journal of Computational Physics* 1985; **59**:308–323.
55. Rhie CM, Chow WL. Numerical study of the turbulent flow past an airfoil with trailing edge separation. *AIAA Journal* 1983; **21**:1525–1532.
56. Sagaut P, Grohens R. Discrete filters for large eddy simulation. *International Journal for Numerical Methods in Fluids* 1999; **31**:1195–1220.
57. Smagorinsky J. General circulation experiments with the primitive equation, I. The basic experiment. *Monthly Weather Review* 1963; **91**:99–165.
58. von Kármán Th. The analogy between fluid friction and heat transfer. *Transactions of the ASME* 1939; **61**: 705–710.

59. Horiuti K. A proper velocity scale for modelling subgrid-scale eddy viscosities in large eddy simulation. *Physics of Fluids A* 1993; **5**:146–157.
60. Kravchenko AG, Moin P, Moser R. Zonal embedded grids for numerical simulations of wall-bounded turbulent flows. *Journal of Computational Physics* 1996; **127**:412–423.
61. Moin P, Kim J. Numerical investigation of turbulence channel flow. *Journal of Fluid Mechanics* 1982; **118**: 341–377.
62. Horiuti K. A new dynamic two-parameter mixed model for large-eddy simulation. *Physics of Fluids* 1997; **9**:3443–3464.
63. Monin AS, Yaglom AM. *Statistical Fluid Mechanics*: *Mechanics of Turbulence*, vol. 1. MIT Press: Cambridge, MA, 1971.
64. Piomelli U. *Large-Eddy and Direct Simulation of Turbulent Flows*. Lecture Notes for the 9th Annual Conference of the CFD Society of Canada, Waterloo, Ontario, 2001.
65. Pope SB. *Turbulent Flows*. Cambridge University Press: Cambridge, MA, 2000.
66. Vreman B, Geurts B, Kuerten H. On the formulation of the dynamic mixed subgrid-scale model. *Physics of Fluids* 1994; **6**:4057–4059.
67. Wang B-C, Bergstrom DJ. An integral type dynamic localization two-parameter subgrid-scale model: formulation and simulation. *International Journal of Computational Fluid Dynamics* 2004; **18**:209–220.
68. Tao B, Katz J, Meneveau C. Statistical geometry of subgrid-scale stresses determined from holographic particle image velocimetry measurements. *Journal of Fluid Mechanics* 2002; **457**:35–78.
69. van der Bos F, Tao B, Meneveau C, Katz J. Effects of small-scale turbulent motions on the filtered velocity gradient tensor as deduced from holographic particle image velocimetry measurements. *Physics of Fluids* **14**: 2456–2474.
70. Horiuti K. Roles of non-aligned eigenvectors of strain-rate and subgrid-scale stress tensors in turbulence generation. *Journal of Fluid Mechanics* 2003; **491**:65–100.
71. Pullin DI, Saffman PG. Reynolds stresses and one-dimensional spectra for a vortex model of homogeneous anisotropic turbulence. *Physics of Fluids* 1994; **6**:1787–1796.
72. Misra A, Pullin DI. A vortex-based subgrid stress model for large-eddy simulation. *Physics of Fluids* 1997; **9**:2443–2454.

